
Masters Theses


Student Theses and Dissertations

Spring 2016

Imaging reinforced concrete: A comparative study of Ground Penetration Radar and Rebarscope

Abhishek Kodi

Follow this and additional works at: https://scholarsmine.mst.edu/masters_theses

 Part of the [Environmental Engineering Commons](#), [Geological Engineering Commons](#), [Geology Commons](#), [Geophysics and Seismology Commons](#), and the [Geotechnical Engineering Commons](#)
Department:

Recommended Citation

Kodi, Abhishek, "Imaging reinforced concrete: A comparative study of Ground Penetration Radar and Rebarscope" (2016). *Masters Theses*. 7509.

https://scholarsmine.mst.edu/masters_theses/7509

This thesis is brought to you by Scholars' Mine, a service of the Missouri S&T Library and Learning Resources. This work is protected by U. S. Copyright Law. Unauthorized use including reproduction for redistribution requires the permission of the copyright holder. For more information, please contact scholarsmine@mst.edu.

**IMAGING REINFORCED CONCRETE : A COMPARATIVE STUDY OF GROUND
PENETRATION RADAR AND REBARSCOPE**

by

ABHISHEK KODI

A THESIS

Presented to the Faculty of the Graduate School of the

MISSOURI UNIVERSITY OF SCIENCE AND TECHNOLOGY

In Partial fulfilment of the Requirements for the Degree

MASTER OF SCIENCE

in

GEOLOGICAL ENGINEERING

2016

Approved by

Neil L. Anderson, Advisor

Evgeniy V. Torgashov

J. David Rogers

© 2016
Abhishek Kodi
All Rights Reserved

ABSTRACT

Geophysical techniques have been playing a very vital role in subsurface imaging in the recent past. Technology has been making it both reliable and convenient to utilize non-destructive geophysics techniques like Ground Penetration Radar, Induction current based Rebarscope, Seismic methods, ERT, etc. The applications range from shallow subsurface investigation of Bridge decks to old tunnels, mapping of rabars in a pre-existing construction and analyzing the concrete strength.

The thesis constitutes of a comparative study and analysis of a Ground Penetration Radar system and a Rebarscope. Individual parameters obtained directly from the study and obtained indirectly from the study shall be analyzed for a better quantitative understanding of their variation and errors to optimize the utility of the instruments individually. Data obtained from both Ground Penetration Radar system and Rebarscope would be compared for accuracy in determining the rebar depth. For the experiments, pre-designed concrete slabs are constructed with rebars at various depths and defects in concrete. Furthermore, a combination of both the instruments is used to minimize errors and to achieve better control over the intrinsic and extrinsic errors of the instruments to undertake real world studies with better dependency.

A calibration, comparative and combination study of Ground Penetration Radar and Rebarscope is important for the very purpose of better understanding of the quality of concrete, especially in its initial stages of degradation. The amplitude variation in the signal and dielectric permittivity of the concrete indicates concrete quality. The study illustrate the superiority of the Ground Penetration Radar system, but in cases of highly varying degradation and construction errors Rebarscope plays key role in accurate depth estimation of the reinforcement rebars. The study highlights some limitations of GPR surveys and proceeds to address the limitations by utilizing a Rebarscope in combination with GPR system.

ACKNOWLEDGMENTS

First off, I would like to express my immense gratitude to Dr. Neil Anderson, my advisor and the chairman of the committee. I greatly appreciate his advice, encouragement and trust in my abilities. I would like to give special thanks to Dr. Evgeniy Torgashov for his invaluable support, cooperation and hands on experience which helped me plenty. Many thanks to Dr. David Rogers, who's been an inspiration and always been helpful with my research.

I would also like to extend my thanks to the faculty members and staff of the Department of Geosciences and Geological and Petroleum Engineering. Thanks to all my colleagues for their collaboration and hard work. Specifically, Aleksey Kamzin and Aleksandra Varnavina for their continuous support.

In addition, I would like to thank Dr. Leslie Sneed for she had a big role in helping me obtain the casted concrete slabs.

Last but not least, all my gratitude to my parents Ravi Shankar and Lakshmi Shankar, sister Sameera, and friends Devika, Avinash, Arun, Ravi Teja, Sujith, Sriram, Raghavendra and many more all around the world, thank you all for your love, support and understanding.

TABLE OF CONTENTS

	Page
ABSTRACT	iii
ACKNOWLEDGMENTS	iv
LIST OF ILLUSTRATIONS	viii
LIST OF TABLES	x
 SECTION	
1 LITERATURE REVIEW	1
1.1 INTRODUCTION	1
1.2 PROBLEM DEFINITION	2
1.3 SCOPE AND OBJECTIVE	2
1.4 CAUSES OF BRIDGE DECK DETERIORATION	3
1.4.1 Chemical Degradation.	3
1.4.2 Poor Design and/or Construction.	5
1.4.3 Temperature Induced Deterioration.	7
1.4.4 Traffic Induced Deterioration.	8
1.5 NONDESTRUCTIVE METHODS FOR INVESTIGATING BRIDGE DECK DETERIORATION.	8
1.5.1 Chain Dragging and Hammer Sounding.	9
1.5.2 Ground Penetrating Radar.	10
1.5.3 Other Non-destructive Evaluation Methods.	12
1.5.3.1 Half-cell potential.	13
1.5.3.2 Infrared thermography	13
1.5.3.3 Seismic methods	13
1.6 DESTRUCTIVE EVALUATION METHODS FOR INVESTIGATING BRIDGE DECK DETERIORATION.	14
1.6.1 Coring.	14
1.6.2 Chloride Ion Concentration Measurements.	14
1.7 METHODS OF BRIDGE DECK REHABILITATION	15

1.7.1 Complete Deck Replacement.....	15
1.7.2 Removal and Replacement of Deteriorated Concrete.....	16
1.7.2.1 Traditional impact removal.....	16
1.7.2.2 Hydro-demolition.....	16
2 CONCRETE SLAB CONSTRUCTION	18
2.1 SLAB 1	18
2.2 SLAB 2 AND SLAB 3	19
3 REBARSCOPE.....	21
3.1 INTRODUCTION	21
3.2 PARTS	21
3.3 MODES OF USE AND RESOLUTION	23
3.3.1 Short mode.....	23
3.3.2 Deep mode	23
3.4 HANDLING THE REBARSCOPE.....	24
3.4.1 Introductory Screen.....	24
3.4.2 Evaluation of Rebar Size.	26
3.4.3 Evaluation of Cover.	27
3.4.4 Statistical Evaluation of Cover.	28
3.5 COVER MAP MENU.....	29
3.6 SCAN MAP MENU	30
3.7 UPLOAD MENU.....	31
4 GROUND PENETRATION RADAR.....	32
4.1 GROUND PENETRATING RADAR TYPES.....	33
4.1.1 Frequency Modulated GPR.....	33
4.1.2 Synthetic Pulse GPR.	34
4.1.3 Pulsed (or Impulse) GPR.	34
4.2 GROUND PENETRATING RADAR ANTENNAS	35

4.3 ELECTROMAGNETIC THEORY PERTINENT TO GPR SYSTEMS	36
5 DATA ACQUISITION AND PROCESSING.....	40
5.1 GROUND PENETRATING RADAR INVESTIGATIONS.....	40
5.2 REBARSCOPE.....	41
5.3 DATA PROCESSING AND ANALYSIS.....	44
5.4 ANALYSIS (PARAMETERS).....	46
5.4.1 Location.	46
5.4.2 Two-way Travel Time.	46
5.4.3 Depth (Apparent and Real).	49
5.4.4 Dielectric Permittivity.....	53
5.4.5 Amplitude.	54
6 CONCLUSION.....	57
BIBLIOGRAPHY	58
VITA	62

LIST OF ILLUSTRATIONS

	Page
Figure 1.1: Chemical corrosion of rebars.....	4
Figure 1.2: De-laminations in the concrete	5
Figure 1.3: General trend of concrete cover related to the rate of corrosion in the rebars.....	6
Figure 1.4: Chloride intrusion in relation to consolidation of cement	7
Figure 1.5: Chain drag technique and the hammer technique for bridge deck assessment	10
Figure 1.6: Simple Ground Penetration Radar system	11
Figure 1.7: PSPA data acquisition.....	13
Figure 1.8: Hydro-demolition.....	17
Figure 2.1: Blue print and slab dimensions	18
Figure 2.2: Slab-1 before pouring concrete	19
Figure 2.3: Both Slab-2 and Slab-3 before casting	20
Figure 2.4: Pre-constructed images of Slab-2 and Slab-3	20
Figure 3.1: Rebarscope parts	21
Figure 3.2: Rebarscope Straps.....	22
Figure 3.3: Range of Rebarscope	23
Figure 3.4: Error ranges based on rebar spacing	24
Figure 3.5: Rebarscope home screen.....	25
Figure 3.6: Main menu	25
Figure 3.7: Size screen and sensor	26
Figure 3.8: Sensor data acquisition	26
Figure 3.9: Sensor with spacer on surface.....	27
Figure 3.10: Screen elements	27
Figure 3.11: Statistical evaluation option.....	28
Figure 3.12: Screen for statistical evaluation of the cover data	29
Figure 3.13: Legend for map cover and ranges.....	29
Figure 3.14: Map navigation	30
Figure 3.15: System display options	30
Figure 4.1: Ground Penetration Radar system structure scan mini	32
Figure 4.2: GPR signal time frequency diagram.....	34
Figure 4.3: Diagram of GPR system processes.....	36
Figure 5.1: GPR data acquisition	40

Figure 5.2: Data acquisition	41
Figure 5.3: Rebarscope data acquisition.....	42
Figure 5.4: Data acquisition of Slab-1 with variable depth.....	43
Figure 5.5: Ground Penetration Radar data.....	44
Figure 5.6: Rebarscope map with data points	45
Figure 5.7: Model of slab and depth parameters	45
Figure 5.8: Two way travel times for Slab-1.....	47
Figure 5.9: Two way travel time for Slab-2	48
Figure 5.10: Estimated depth of rebars	50
Figure 5.11: Depth of rebars for Slab-2.....	51
Figure 5.12: Slab-2 depth plots	51
Figure 5.13: Slab-3 rebar depth estimated and real values.....	52
Figure 5.14: Amplitude and moisture contents relationship	54
Figure 5.15: Amplitude vs deterioration relationship	55
Figure 5.16: Sensor angle vs correction factor	55

LIST OF TABLES

	Page
Table 1.1: Average dielectric permittivity constants for different mediums.....	11
Table 5.1: Slab 1 two way travel time.....	47
Table 5.2: Slab 2 two way travel time for rebar reflections	48
Table 5.3: Slab 3 two way travel time for the rebar reflections	49
Table 5.4: Slab 1 rebar depths	49
Table 5.5: Depth values comparative	50
Table 5.6: Slab 3 rebar depths	52
Table 5.7: Dielectric permittivity's estimated for the three slabs	53

1 LITERATURE REVIEW

1.1 INTRODUCTION

Engineering construction is based predominantly on reinforced concrete. Dominant efforts have been put into developing the theoretical and practical aspects of designing and constructing. Over the span of time the infrastructure grows old and eventually fails to keep up with the purpose it serves. Regular inspection of engineering structures is essential for an assessment of their robustness, especially for the purposes of maintenance & modification, so as to keep it functional within the prescribed safety norms. Failure to identify signs of deteriorating engineering structure can lead to catastrophic results especially when dealing with critical infrastructure like roads, bridges, reservoirs, buildings, dams, etc.

Until late 1980's and early 90's the post construction inspection process was limited to visual features on the exterior like the surface manifestations or signature manifestation in terms of audible knocking change or pre-embedded sensors. In a relative sense the protocols were primitive and for elaborate assessments the process was expensive. Through the course of technological evolution, effective techniques have come into limelight. Geophysics has risen to address the challenges through multitude of tools. One dominant tool being, electromagnetic waves based system that can now be used to image the interior of engineering structures. The invisible elements of an engineered structure like, the interior of a bridge deck, the walls of a building, etc. can be monitored through electromagnetic waves. This technology is a quantum step forward, in comparison with the techniques employed in the past, at a highly viable economic cost. Though these technologies are new and still in the process of providing comprehensive results they do add new dimensions to our understanding. Moreover, they have built a launch pad for the technology to evolve into a more conclusive one in the very near future. Rise of these technologies and aging infrastructure puts them in a vital spot in today's engineering world.

Transportation infrastructure is a lifeline to any society, with extensive utilization of these facilities day in and day out a big challenge for transportation departments is to not just provide the infrastructure but maintain and test their roads and bridges with minimal public inconvenience. In this arena, Geophysics is playing a key role in optimized assessment of bridge decks and is making it possible to act upon reliable data to preserve and make optimal use of bridges. Engineering structures like most functional elements fail to fulfill their function based on their weakest link in the design, which generally for bridges are their decks. It's the bridge

decks that are exposed to maximum wear and tear. They are affected by the physical wear and tear through movement of vehicles, debris, sunlight, weather conditions, etc. At a chemical level, exposure to de-icing agents, chemicals remnants from vehicle emissions, water and any exposure through atmosphere can cause damage over time. Thus, bridges are not only subjected to physical deterioration but also to chemical.

1.2 PROBLEM DEFINITION

Geophysical instruments like Ground Penetration Radar and Rebarscopes are utilized to estimate the depth, condition and properties of the rebars and extrapolated for the concrete. The straightforward method of inspection is to take core samples which may lead to destruction and has multiple limitations such as location, cost, public convenience and comprehensiveness in assessment. Non-destructive methods are the preferred techniques and geophysical tools are the coveted methods for a cost-effective, comprehensive and reliable understanding. But geophysical tools like Ground Penetration Radar and Rebarscope are not direct evaluators of the concrete but rather the embedded rebars. Through the variation in the properties obtained for the rebars, the information can be extrapolated for the concrete condition between the source and the rebars. Parameters like the amplitude loss and apparent depth of rebar at the location are indicative of the concrete properties. Variations in these parameters is critical and may lead to inaccurate extrapolation which may in turn lead to misinterpretation of the concrete quality. The economic aspects are very crucial for concrete constructions as the ASTM standards need to be met at all times, which could become an economic burden. To roughly estimate, rehabilitation of a minor bridge costs up to \$250,000 which in no way is a justifiable expense for any institution without strong conviction of the necessity. This would vary for an indoor concrete construction and costs could fluctuate based on design changes or reconstruction.

Now that we have established the importance of accuracy and minimization of errors in bridge decks and generally in concrete construction, we need to address the accuracy and error range of the geophysical tools, techniques, and applied parameters. We need to work towards making the results reliable as well as optimal by minimizing errors.

1.3 SCOPE AND OBJECTIVE

The objective of the dissertation is to employ geophysical techniques of Ground Penetration Radar and Rebarscope in a controlled environment to obtain a good understanding of the parameters that affect our interpretation of the concrete and find ways to minimize them. One

aspect of the thesis is to test the parameters and the error ranges of the parameters. To test the instruments, specially pre-designed, concrete slabs with steel reinforcements (rebars). One with rebars placed at variable depths and a second block has rebars placed at constant depth with some obstructions mimicking concrete defects. As the Ground Penetration Radar and Rebarscope are indicative of the rebar locations, the precision of the instruments would be the first objective. Then a comparative study between the Rebarscope and the Ground Penetration Radar would be conducted. The final stage would be to use the instruments in combination, to obtain the best results with minimized error ranges.

Bridge decks experience harsh conditions that lead to their deterioration. In order to monitor the health of bridge decks, transportation officials commonly use both non-destructive and destructive test methods. Once a bridge deck reaches a certain level of deterioration, it will require repair or replacement. This section discusses causes of bridge deck deterioration, along with evaluation and repair methods.

1.4 CAUSES OF BRIDGE DECK DETERIORATION

The causes of bridge deck deterioration are placed into four main categories for this thesis. The four main categories are degradation caused by chemicals, poor design and/or construction, thermal changes, and degradation induced by traffic. All of these deterioration mechanisms are unique and should be taken into consideration when evaluating a bridge deck.

1.4.1 Chemical Degradation. According to the Portland Cement Association (PCA), “corrosion of reinforcing steel and other embedded metals is the leading cause of deterioration in concrete” [2]. Chloride ions found in de-icing chemicals and some admixtures can accelerate the rate of steel corrosion, resulting in a decreased service life of the bridge deck. Even though careful design and construction practices can limit the intrusion of de-icing chemicals and extend the life of a bridge deck, the concrete will eventually crack and allow these chemicals to come in contact with the reinforcement. It is also important to recognize that many bridges constructed during the 1960s and 1970s that are still in service were not built with the design standards that transportation agencies use today. Currently, bridges constructed during the 1960s and 1970s are structures for which Department of Transportation (DOT) are most interested in obtaining data through non-destructive methods for monitoring and rehabilitation planning. Therefore, it is crucial to understand the main deterioration mechanism that affects bridge decks especially in states like Missouri.

According to PCA, common de-icing chemicals used on roadways include sodium chloride, calcium chloride, magnesium chloride, and potassium chloride [3]. Although these chemicals greatly aide in keeping the roadways navigable during snow and icy conditions, by reducing the freezing point of water, they cause substantial damage to highway infrastructure. In order for corrosion of steel to occur, there has to be at least two electrically connected metals or two locations of a single metal at different energy levels acting as the anode and cathode, and an electrolyte to connect the two. The anode is the location where the corrosion occurs, or where the loss of cross section is noticed. The cathode is the area where steel is not consumed. Moist concrete acts as the electrolyte. Figure 1.1 below illustrates the corrosion mechanism [2].

Concrete naturally protects the steel reinforcement from corrosion because of its high alkalinity with a pH between 12 and 13. This high pH allows a thin oxide layer to form on the steel and prevents metal atoms from dissolving. The oxide layer does not stop corrosion, but it does reduce the corrosion rate enough that it is insignificant [2]. Chlorides present in the concrete from de-icing chemicals and possibly the concrete mixture can break through this passive layer and initiate higher corrosion rates. According to the Federal Highway Administration (FHWA), it is not fully understood how chloride ions break down the passive layer [4]. Once the passive layer is broken, oxygen and water can reach the steel allowing corrosion to occur. Corrosion products from the steel occupy a volume of three to six times that of original steel, inducing large tensile stress in the concrete [4]. If the tensile strength of the concrete is exceeded, a horizontal crack called a delamination will occur.

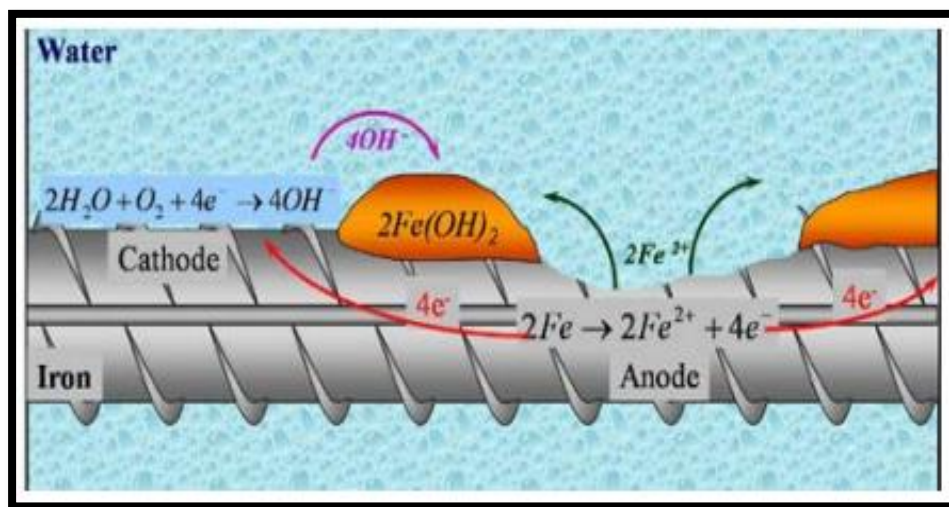


Figure 1.1: Chemical corrosion of rebar (www.cement.org)

According to the American Concrete Institute (ACI), a delamination is defined as “horizontal splitting, cracking, or separation within a slab in a plane roughly parallel to, and generally near the upper surface” [5]. De-laminations can cause an increased rate of corrosion as well as visible deterioration on the bridge deck surface such as spalling and potholes, as illustrated in figure 1.2.

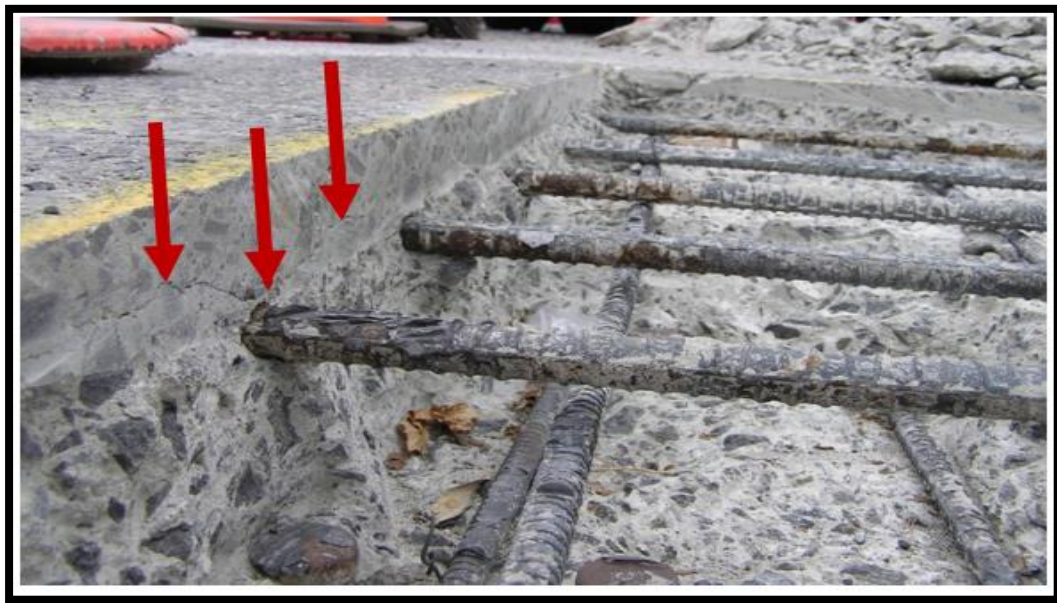


Figure 1.2: De-laminations in the concrete (www.ndtoolbox.org)

1.4.2 Poor Design and/or Construction. Poor bridge deck design and construction can cause accelerated deterioration. One of the most effective ways to decrease the rate of corrosion is to ensure that the steel reinforcement has adequate concrete cover. MODOT currently has a minimum top reinforcement clear cover requirement of 72.75 inches, with a preferred cover of 3.0 in. [7]. The greater the clear cover, the longer it will take for chlorides to reach the steel and initiate corrosion. Figure 1.3 below illustrates how increased concrete cover on reinforcement can greatly reduce the corrosion rate of the steel reinforcement [8]. The model presented in the Figure was generated using a constant humidity and temperature of 75% and 20°C (68°F), respectively.

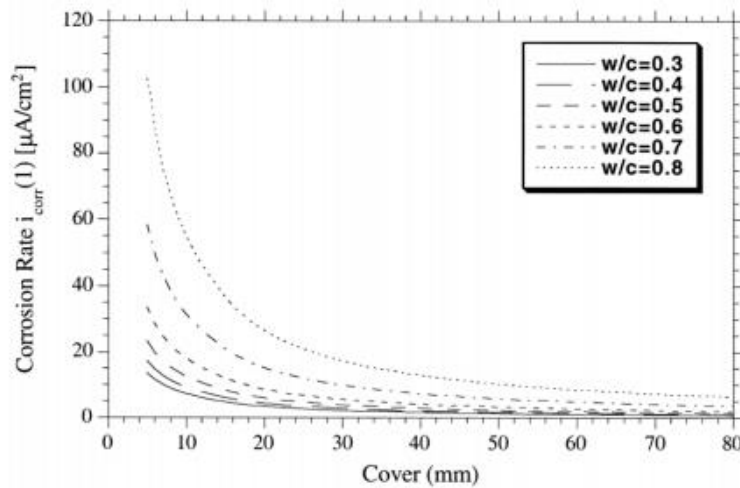


Figure 1.3: General trend of Concrete cover related to the rate of corrosion in the rebars

Another important consideration in the deterioration rate of steel-reinforced concrete bridge decks is the concrete mixture used. Figure 1.3 above illustrates that mixtures with lower water-to-cement ratios (w/c) have lower corrosion rates than those with higher w/c ratios. The material being used in the concrete mixture is also important to the durability of the bridge deck. For example, alkali-aggregate reactions (AAR) are an important consideration while specifying aggregates for use in concrete. AAR is a chemical reaction in concrete between hydroxyl ions of the alkalis from hydraulic cement and certain constituents of some aggregates [9]. Although uncommon in Missouri, deterioration due to AAR can greatly decrease the life of a bridge deck. AAR causes the concrete to expand and crack, allowing for water and de-icing chemicals to reach the reinforcing steel rapidly. The reaction can eventually cause failure of the concrete. AAR can be prevented by using a combination of aggregate and cement that will not react. Placement and consolidation of the concrete can have a significant impact on the deterioration rate of the bridge deck. Concrete should be properly consolidated to ensure that there are no large voids present in the deck. If the concrete is not well consolidated, these voids can cause accelerated deterioration as they trap water and de-icing chemicals. Studies completed at the Arabian Gulf University showed that the amount of consolidation can significantly affect the rate of chloride intrusion as illustrated in Figure 1.4 below [10].

After the concrete placement of a bridge deck is complete, it is critical that the deck is cured properly. The quality of curing greatly affects the quality of the top layer of concrete in the bridge deck, which is closely related to the durability and longevity of the deck. Proper curing can greatly reduce initial cracking and permeability of the concrete. Shrinkage cracks caused

from improper curing can allow de-icing chemicals to penetrate the reinforcing steel at a greater rate than for un-cracked concrete. According to PCA, standard recommendations for curing bridge decks consist of moist curing for a minimum of seven days for concrete mixtures containing only Portland cement and as long as 14 days when supplementary cementitious materials are used [12].

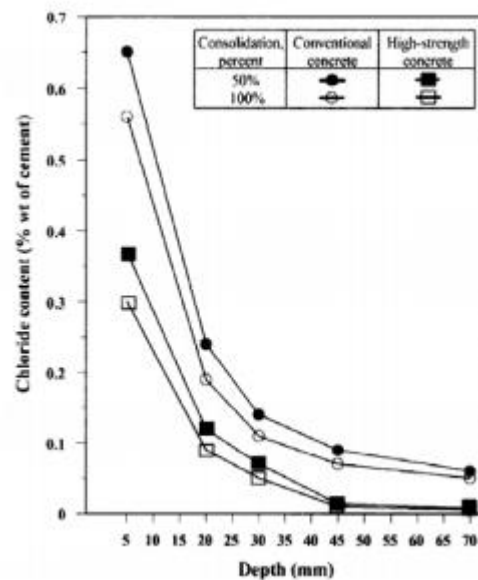


Figure 1.4: Chloride intrusion in relation to consolidation of cement

1.4.3 Temperature Induced Deterioration. Temperature changes can induce deterioration of the bridge deck, mainly through the creation and propagation of cracks. Any type of crack in the concrete can allow aggressive agents such as de-icing chemicals to penetrate the deck causing damage to either the concrete itself or the reinforcing steel [13]. Freezing and thawing cycles are one form of temperature change that can cause deterioration of bridge decks. Solutions in the pores of the concrete expand during a freezing event and exert high pore pressures. If the tensile strength of the concrete is exceeded, it will result in cracking [14]. There are also other causes of temperature induced deterioration. When de-icing agents are placed on the bridge deck, they decrease the freezing point of water and allow ice and snow to melt. This process draws heat from the concrete and chills it, which can act like a cold shock. The pore water on the concrete surface then freezes and can cause cracking if internal stress exceeds the tensile strength of the concrete [15]. Damage from temperature differences can also occur due to layered freezing. Layered freezing is caused due to the de-icing agent concentration and temperature gradients within the concrete. The surface layer has a relatively low temperature and

a high de-icing agent concentration. The interior of the concrete has a relatively low de-icing agent content and higher temperature. The layer in between the surface layer and interior freezes at lower temperatures than the other two, which can cause high pressures on the surface layer. If the stresses exceed the tensile strength of the concrete, it will crack [15].

1.4.4 Traffic Induced Deterioration. Traffic load can have an impact on the deterioration of bridge decks. According to a report by the Iowa Department of Transportation “various surveys indicate that highway bridges are subjected to vehicular load levels and combinations far in excess of those for which they were designed for” [15]. Damage typically caused from overloading includes hair line cracks, bending, and splitting or shear cracks [15]. Traffic induced damage was observed on several concrete bridge decks with bituminous overlays. Typical damage included rutting and shoving of the asphalt, especially where traffic stops and turns. The asphalt overlay can also de-bond from the concrete, allowing moisture with and/or without chlorides to be trapped in the de-bonded region, allowing for further deterioration [16]. Even though the deterioration of the asphalt layer does not necessarily reflect the strength or deterioration of the concrete bridge deck, it is important to use non-destructive evaluation techniques that are sensitive to all layers on the bridge decks because asphalt deterioration could influence the interpretation of results.

1.5 NONDESTRUCTIVE METHODS FOR INVESTIGATING BRIDGE DECK DETERIORATION.

Non-destructive evaluation (NDE) methods are simply defined as methods of detecting flaws or deterioration without damaging the material. Basic forms of NDE methods used for bridge decks include visual inspection and sounding by chain dragging or hammer sounding. More advanced methods, such as Ground Penetrating Radar (GPR), are being widely used as they are further researched on and better understood. It is important to consider the strengths and limitations of each technology, and in many cases the use of a combination of techniques to accurately determine bridge deck deterioration.[] Visual Inspection. The first step in evaluating the condition of a bridge deck is a visual inspection [17]. A careful visual inspection of a bridge deck involves examining the top and bottom of the bridge deck. Important characteristics to take note of during an investigation include concrete stains, cracks, localized depressions, spalling, and scaling. Rust stains on the concrete are indicators that the steel reinforcement may be corroding, but sometimes it can be a result of other actions such as ferrous sulphide inclusions in the aggregate or rusting of form ties [17].

Cracks are precursors of deck deterioration and are one of the most important features to document. Cracks can eventually allow de-icing agents and water to reach the reinforcing steel, accelerating deterioration of the deck. It is also important to document the orientation of the crack as either longitudinal, traverse, diagonal, or random. This can help determine the cause of the cracking. Typically, crack widths and depths are not measured on a bridge deck. However, if desired, crack widths can be measured by instruments such as a crack width comparator card [18], or a hand-held crack comparator microscope. Localized depressions can indicate areas where the concrete has deteriorated below the surface. Spalling occurs when the surface of the concrete pops out and leaves the aggregate exposed. Scaling occurs when the surface of the concrete flakes off. Even though visual inspection is a very common method used to evaluate bridge decks, it is very subjective. A study completed by the Federal Highway Administration (FHWA) shows that different inspectors have substantially different visual ratings of the same bridge decks.

1.5.1 Chain Dragging and Hammer Sounding. Chain dragging and hammer sounding techniques are commonly used to locate de-laminations in bridge decks. ASTM D4580-12 describes the process that should be followed for the sounding of bridge decks [21]. Sounding is not recommended for bridge decks overlaid with bituminous mixtures, but can be used for bridge decks that have been overlaid with Portland cement concrete mixtures. The procedure listed in the ASTM standard includes laying out a grid system on the bridge deck, followed by dragging chains over the deck surface. Areas that are de-laminated have a dull or hollow sound when the chain is drug across. Areas that are believed to be de-laminated are outlined on the deck surface, and a map is prepared indicating the location of the de-laminations with respect to the grid lines. A steel rod or hammer can be substituted for chains as long as it produces a clear ringing sound when dragged or tapped over a pristine (non-delaminated) concrete and a dull or hollow sound over de-laminated concrete [21]. Figure 1.5 below shows a chain dragging and hammer sounding [22].

Chain dragging is the second most widely used method in the United States to assess the condition of bridge decks because it is relatively simple, economical, and quick to perform [17]. Even though it is widely used, sounding techniques are susceptible to inconsistencies due to subjective interpretations an inspector makes during the survey [23]. Sounding methods can only detect de-laminations when they have progressed to the point where major rehabilitation is required [24].



Figure 1.5: Chain drag technique and the hammer technique bridge deck assessment (www.ndtoolbox.org)

1.5.2 Ground Penetrating Radar. Ground Penetrating Radar (GPR) is a rapid non-destructive testing method that utilizes electromagnetic (EM) waves that can be used to locate buried objects inside the bridge deck such as steel reinforcement, wire mesh, or other interfaces in the structure [25]. GPR has many applications, such as condition assessment of bridge decks and tunnel linings, pavement profiling, mine detection, archaeological investigations, geophysical investigations, and borehole inspections [16]. “GPR was originally developed for overlaid decks since access to the concrete surface via traditional methods is limited” [26]. A GPR antenna transmits small high-frequency EM pulses into the structure of interest. A portion of the energy is reflected back to the antenna from reflectors such as reinforcing bars or any other change in the material. The remaining energy continues to propagate further into the structure, and some energy is continually reflected until it is diminished. A receiver measures the amplitude and two-way travel time of the reflected signals. Figure 1.6 below illustrates how GPR works.

GPR responds to variations in electrical properties of the materials making up various interfaces in a bridge deck. Material interfaces are typically recognizable with the GPR results because the materials on either side of the interface have different electrical conductivity and dielectric constants [16]. These properties affect the ability of GPR energy to penetrate the material, and the speed at which the GPR waves travel through the material. Table 1.1 below lists the dielectric constants of various materials [28]. Notice that water has a relatively high dielectric constant compared to concrete.

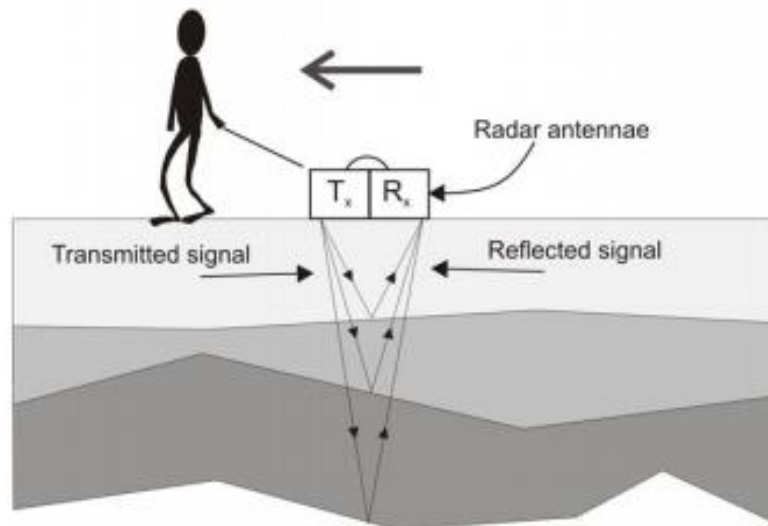


Figure 1.6: Simple Ground Penetration Radar system (www.environmental-geophysics.co.uk)

Table 1.1: Average dielectric permittivity constants for different mediums
(www.ndtoolbox.org)

Air	1	Sand	4-6
Water (fresh)	81	Gravel	4-7
Ice	4	Clay	25-40
Asphalt	4-8	Silt	16-30
Concrete	8-10	Silty sand	7-10
Crushed base	6-8	Insulation board	2-2.5

Due to the large difference in dielectric constant between water and concrete, moist concrete with high free chloride ions (or other conductive materials) attenuates the GPR signal and creates a longer two-way travel time than that of dry concrete [28]. Therefore, deteriorated regions that are filled with moisture and conductive materials, such as chloride ions, can be located. Electromagnetic waves cannot penetrate into metals; therefore steel reinforcing bars are excellent reflectors of EM waves. ASTM (D6087) describes the use of GPR for the evaluations

of bridge decks with and without asphalt overlays [29]. Two methods of analysing GPR results are presented in this standard.

1. Deterioration measurements at the top reinforcing steel using the bottom deck reflection attenuation technique
2. Deterioration measurements at or above top reinforcing steel using top reinforcing reflection attenuation technique.

Even though there are two analysis methods, typical GPR surveys utilize the second method, which uses the reflection amplitude from the top layer of reinforcement to analyse results. The sample GPR results from a bridge deck [30]. The hyperbolas in the image represent reflections from the reinforcing bars. The boxed area shows a section of the bridge deck that is predicted to be deteriorated, as indicated by signal attenuation and varying apparent depths of reinforcing bars.

Some limitations of GPR include:

1. GPR can determine the locations of de-laminations only if they are filled with water or epoxy-impregnated.
2. Extreme cold weather can negatively influence GPR results. Studies by the FHWA state that frozen water is relatively transparent to EM waves in the frequency range typically used for bridge scans [33].
3. De-icing agents can limit the ability for GPR signal to penetrate the deck.
4. GPR cannot provide any information on mechanical properties of concrete.
5. GPR cannot provide any information about the presence of corrosion, corrosion rates, or reinforcing bar section loss.
6. Other test methods may be more cost-effective than GPR, especially for smaller structures.
7. The design of new GPR systems is limited by FCC restrictions on transmitting power output and the pulse repetition rate.
8. GPR results typically benefit from being correlated or validated by some other NDE methods or limited destructive sampling such as core extraction, or chloride sampling and testing.

Although these limitations exist, GPR is still a beneficial tool that can be used in combination with other evaluation techniques to evaluate bridge deck deterioration.

1.5.3 Other Non-destructive Evaluation Methods. Many other methods exist that can be applied to detecting bridge deck deterioration. Although methods in this section are not discussed in other sections of this thesis, they are still evaluation tools that can be used in bridge deck condition assessments. In this section, several non-destructive testing methods that can be used for bridge deck condition assessments are briefly summarized.

1.5.3.1 Half-cell potential. Half-cell potential (HCP) measurements are used to evaluate the active corrosion in steel reinforcement. The potential difference between reinforcement and a standard portable half-cell is measured, which can be used to determine the probability of active corrosion. Some limitations of the device include difficult interpretation due to numerous material properties that can influence measurements, and required pre-wetting of the test object to allow galvanic coupling [16].

1.5.3.2 Infrared thermography. Infrared thermography (IR) utilizes temperature variations of the bridge deck surface to predict areas of deterioration. Voids, cracks, delaminations, and concrete disintegration can be located using IR. Sections of the bridge deck that contain concrete with different material properties, such as density, thermal conductivity, and specific heat capacity have different rates of heating and cooling, therefore these differences can be located [16].

1.5.3.3 Seismic methods. Seismic methods can be used to detect bridge deck deterioration. Two methods discussed in this section are impact echo (IE) and ultrasonic surface-wave (USW). Both of these techniques are utilized in the Portable Seismic Property Analyser (PSPA). The PSPA is shown in Figure 1.7 below.

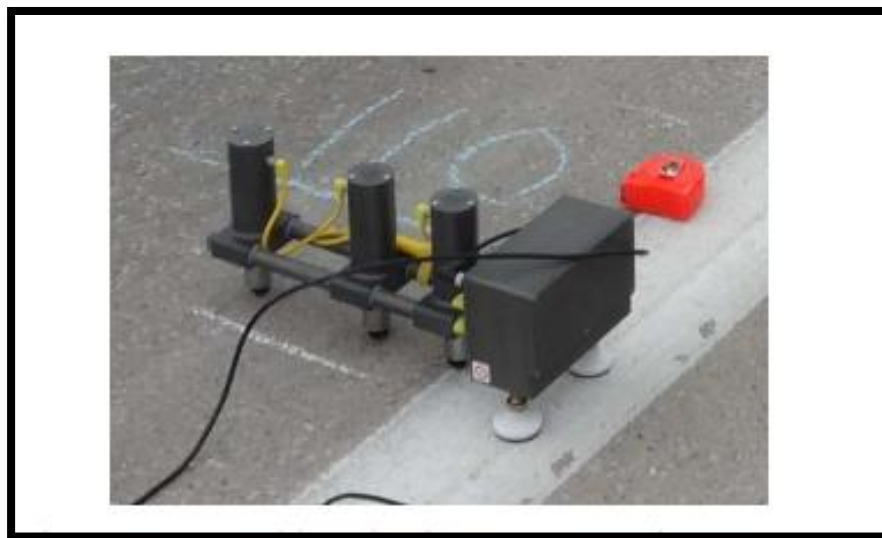


Figure 1.7: PSPA data acquisition

The IE method is used to detect and assess de-laminations, evaluate vertical cracks, and evaluate materials, such as concrete. According to Gucunski, IE is primarily used to identify the

position of wave reflectors in the bridge deck using the return frequency spectrum [15]. During the USW test, the surface material is impacted using a high frequency source. The time domain signals are recorded and then processed to obtain dispersion 20 curves, which are phase velocity vs. wavelength or frequency. Current USW devices automatically process this data. From the USW test, elastic modulus profiles can be generated [16].

1.6 DESTRUCTIVE EVALUATION METHODS FOR INVESTIGATING BRIDGE DECK DETERIORATION

Destructive evaluation techniques are commonly used by transportation officials to monitor bridge decks and plan for repairs and rehabilitations. Two methods discussed in this section include coring and chloride ion concentration testing. Both methods provide localized information about the condition of bridge decks, but they can also be used to validate the results of NDE methods which typically cover more area of the bridge deck.

1.6.1 Coring. Extracting concrete cores from bridge decks is an accurate method to assess localized areas of a bridge deck. ASTM C 42 describes a procedure that can be followed to extract cores from concrete [35]. Core specimens are extracted perpendicular to the concrete surface in the area of interest. Cores are typically taken from areas where distress is noticed to determine the cause of the deterioration. Typically a simple visual inspection is performed on the cores after extraction. ASTM C 856 can be followed if a petrographic analysis is desired [36]. Although coring does provide accurate data, and there are many tests that can be performed on the extracted cores, there are some limitations. Coring provides data for a very small percentage of the bridge deck, and typically transportation officials limit the amount of coring to ensure the strength and durability of the deck. Core extraction and analysis can be expensive because road crews are required to extract the cores, along with trained experts to perform the laboratory analysis. Also, lane closures are required while road crews perform the core extraction and fill the core holes. These core holes can also create weakened zones in the deck and allow moisture and de-icing salts to penetrate to the reinforcing steel if not properly filled.

1.6.2 Chloride Ion Concentration Measurements. Chloride ion concentration tests are commonly performed by many transportation agencies to determine the level of chloride intrusion into the bridge deck. Measurements are taken at different levels within the deck, providing a chloride ion concentration profile. If the concentration is high enough near the reinforcing bars, corrosion can result as the protective passive layer of the reinforcement is broken. There are two types of tests that can be performed to determine chloride ion contents. The first test determines the acid-soluble chloride ion content. The acid soluble chlorides include

chlorides present in the cement. ASTM C1152 can be followed to determine the acid-soluble chloride content [37]. Water-soluble chlorides are the other form of chloride ions that can be measured in bridge decks. They are known to lead to the initiation or acceleration of corrosion in metals [38]. These chloride ions can be a result of de-icing chemicals. ASTM C1218 can be followed to determine the amount of chloride ions present in concrete [38]. Samples for testing can be obtained either from cores extracted from the deck, or directly from the bridge deck. If cores are used, vertical sectioning and pulverization is required before the samples can be tested. If the samples are removed directly from the bridge deck, a rotary hammer can be used to pulverize the concrete, and then the sample can be removed directly from the deck. In this process, samples are taken at specific depth increments, with cleaning of the sampling hole using a vacuum or compressed air in between samples. Pulverization using, rotary hammers and sample extraction for chloride ion determination [23]. Although chloride ion testing is commonly used to determine the likelihood of the steel reinforcement corroding, the exact threshold values for corrosion are difficult to determine [39]. According to Kepler, the concentration of chloride ions at the corrosion threshold is dependent on the ratio of chloride ions to hydroxide ions, however it is not generally presented in this way [39]. In this thesis, a threshold value of 0.15% water soluble chloride ions by weight of cement will be used. This value comes from a study conducted by the FHWA [2].

1.7 METHODS OF BRIDGE DECK REHABILITATION

Departments of transportation have several methods that they use to repair and rehabilitate their bridge decks. Typically the most cost effective method is that chosen by transportation officials. If the deck is in very bad shape and the substructure is in good shape, a complete deck replacement is considered. In other cases, the deck surface may have deterioration that can be repaired at a lower cost than a complete replacement. Common deck repair strategies used by transportation officials are discussed in this section.

1.7.1 Complete Deck Replacement. In some cases, transportation officials determine that a complete bridge deck replacement is more cost effective than rehabilitation. When a deck replacement occurs, the existing deck is completely removed from the substructure of the bridge, and then it is replaced. In 2012, MoDOT completed their Safe and Sound project, in which 248 bridges were rehabilitated in 3.5 years, most of which consisted of complete deck replacements [40]. The average length of bridge closures during this project was 46 days, which also included 554 bridges that were completely replaced [41]. Whenever a bridge deck is replaced, it is critical that the closure time be as short as possible to ensure traffic disruption is minimized. Therefore,

there are many construction methods available that can be considered in order to decrease the construction time of a bridge deck. One of those methods is to use precast pre-stressed panels. These panels can either be partial depth or full depth. MoDOT used full depth precast segments to replace a 1698 ft. bridge deck in 2004. The construction method 24 used closed the bridge Sunday through Thursday nights from 7 PM to 7 AM from Memorial Day to Labor Day 2004, allowing the bridge to be open during heavy traffic periods [42].

1.7.2 Removal and Replacement of Deteriorated Concrete. In some cases, transportation officials find it cost effective to repair deteriorated bridge decks rather than replace them. The level and type of repair varies for each case. There are two common methods to remove the loose and deteriorated concrete, traditional impact removal, and hydro demolition.

1.7.2.1 Traditional impact removal. The most common way to remove deteriorated concrete during the rehabilitation of a bridge deck is to use impact sources, such as jackhammers, to break up the concrete. The repair process starts with a deck sounding using chains and/or hammers that sound deteriorated are marked. Rectangular saw cuts are made around the deteriorated area. Jackhammers are then used to break apart the deteriorated concrete. After the concrete is removed, sandblasting of rusty or dirty reinforcing steel is required. Fresh concrete is then placed into the hole and allowed to cure before reopening to traffic. Concrete used for such patching operations is typically designed for early strength development, which in some instances can lead to early deterioration caused by shrinkage cracking [43].

1.7.2.2 Hydro-demolition. Hydro-demolition is increasing in popularity for the use of bridge deck rehabilitations. It provides several advantages over traditional impact removal techniques. Hydro-demolition utilizes a high pressure water jet stream with pressures in the range of 14,000 to 20,000 psi [44]. Prior to hydro-demolition, the deck must be scarified by using a milling machine. The hydro-demolition machine is then calibrated to remove all unsound concrete plus a little bit more (about 0.5 in.) into sound concrete. Removal of deteriorated concrete may include concrete that is spalled, cracked, delaminated, chloride contaminated, carbonated, or damaged by fires or cycles of freezing and thawing [44]. The machine typically removes the material in one pass, but if needed a second pass can be made. Figure 1.8 below shows a hydro-demolition machine being used to break apart deteriorated concrete. A vacuum is then used to remove all debris from the deck while it is still wet. The deck is then sounded, and any deteriorated concrete that still remains is removed with a jackhammer.



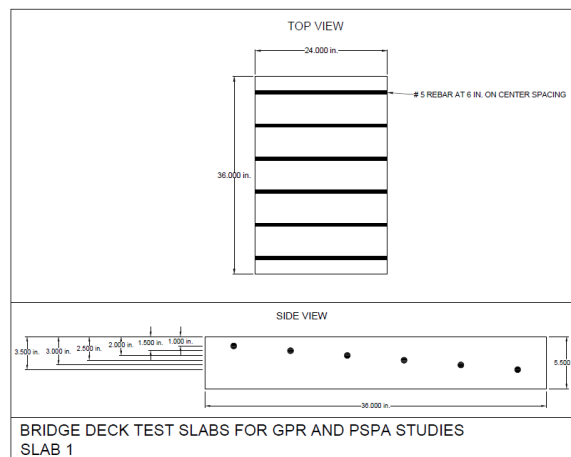
Figure 1.8: Hydro-demolition (www.flickr.com)

Hydro-demolition Machine [45] is a faster, cleaner, and better way to remove deteriorated concrete from bridge decks than traditional impact methods [46]. The hydro-demolition process eliminates the need for saw cuts, sandblasting, and individual patching of deteriorated areas. Hydro-demolition does not induce micro fracturing like impact methods do, therefore the repairs are expected to last longer than when using impact methods [46]. MoDOT has experienced a lot of early deterioration on bridge decks rehabilitated using traditional impact methods, which they concluded is due to the micro fracturing caused by such methods [46]. After the hydro-demolition process, the concrete surface is sufficiently roughened to enhance the bond and help ensure composite action between the base concrete and the repair material [44]. After the deck is free of debris, a latex modified concrete overlay is then placed on top of the existing concrete.

2 CONCRETE SLAB CONSTRUCTION

2.1 SLAB 1

The first Slab was constructed with rebars embedded at various depths in the concrete. The cast was made to get an understanding of the Attenuation of the GPR signal and its effect on depth location of the Rebarscope. The layout of the slabs is presented below. The rebars were placed after the depth of 1 inch and consecutively after every half an inch. Figures 2.1 illustrates the blueprint and the slab dimensions and Figure 2.2 shows the slab before pouring the concrete.



Length (ft)	3.0
Width (ft)	2.0
Height (in)	5.5
Total Volume of Concrete (ft ³)	2.75
Rebar Layout	
Longitudinal Size	N/A
Number of Longitudinal Bars per Layer	0
Number of Longitudinal Layers	0
Linear Feet of Longitudinal Bars Total	0
Transverse Size	#5
Number of Transverse Bars per Layer	6
Number of Transverse Layers	1
Linear Feet of Transverse Bars Total	12

Figure 2.1: Blue print and slab dimensions (courtesy Aleksey Khamzin)



Figure 2.2: Slab-1 before pouring concrete (courtesy Aleksey Khamzin)

2.2 SLAB 2 AND SLAB 3

Both the Slabs 2 and Slab 3 are identically designed but the fundamental difference lies in between them as one of them is a control slab with no induced defects and the other Slab(3) was designed to evaluate and understand the modification of geophysical instrument signal would react to de-laminations and presence of other materials in the concrete. The slab has two sets of parallel rebars and two such layers. It is better illustrated in image below Figure 2.3 and the slab is 5 feet long and 3 feet wide.

In the longitudinal side the rebars are of size #4 , whereas the transverse size #5 rebars. The concrete slab has its first layer of transverse rebars at the depth of 1.875 inches. The slab had multiple materials instilled in it such as to generate defects in concrete as shown in Figure 2.4.



Figure 2.3: Both Slab-2 and Slab-3 before casting



Figure 2.4: Pre-constructed images of Slab 2 and Slab 3

3 REBARSCOPE

3.1 INTRODUCTION

The James Instruments Rebarscope utilizes the latest in eddy current sensing and micro-processor technology to accurately locate, determine the depth of, and estimate the size of metal objects in concrete. The eddy current sensor is specifically designed to react to the outer surface of the metal object only. It is uninfluenced by small particles in the concrete, whether the concrete is fresh or hardened, wet or dry.

The Rebarscope as illustrated in figure 3.1 and figure 3.2, it has built-in test modes for rebar/post tension cable, conduit and copper pipe. The sensor allows the unit to locate both ferrous and nonferrous metals in concrete. The user is aided by using a graphic bar in the display, and an audio tone to quickly and accurately locate metal objects. Overall, it's a simple to use highly effective piece of equipment.

3.2 PARTS

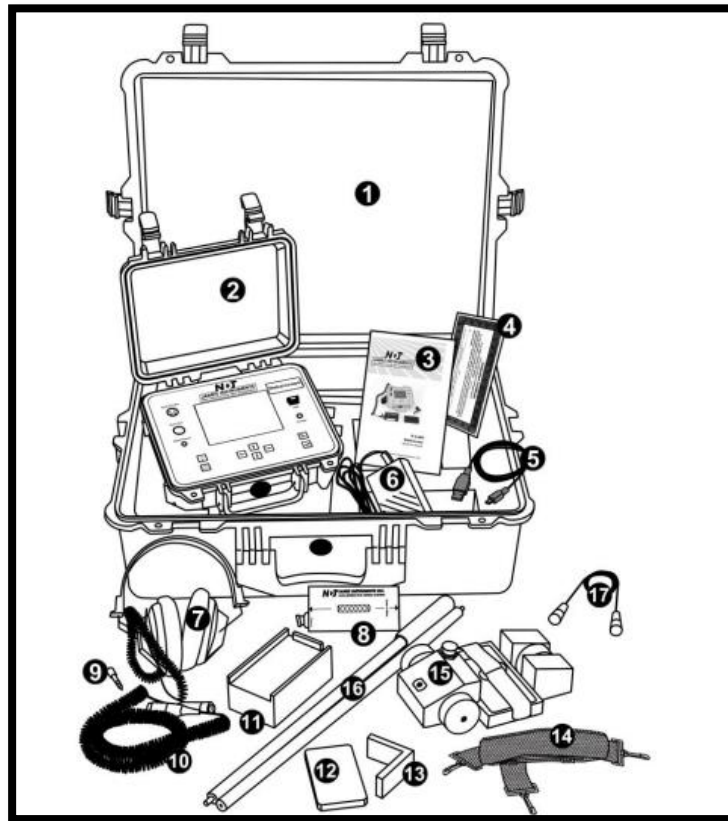


Figure 3.1: Rebarscope parts

1. Case – Used for carrying the Rebarscope and accessories.
2. Rebarscope Instrument – Rebar locator encased in a durable protective case.
3. Instruction Manual – Operating instructions for Rebarscope.
4. Calibration Certificate – Certificate to confirm that the instrument has been calibrated to meet or exceed published specifications.
5. USB Cable – Serial cord used to connect the Rebarscope to a PC to upload data.
6. AC Power Adapter – Used to power the Rebarscope and recharge the unit.
7. Headphones – Used in noisy environments.
8. Sensor Probe – Shows direction of rebar.
9. Phone Jack – For headset.
10. 8' Coiled Cable – Used with the Sensor Probe.
11. A 5/8" Spacer Block – Used to add space in lower cover situations.
12. 3/8" Spacer Block – Used for sizing feature.
13. Locating Template – Used for sizing feature.
14. Support Strap – Used to secure the Rebarscope to the user during testing.
15. Scan Cart – (opt.) Comes with Complete system only.
16. Scan Cart Extension Poles – (opt.) Used to guide Scan Cart
17. Scan Cart Cable – (opt.) Yellow cable used to connect Scan Cart to main unit.

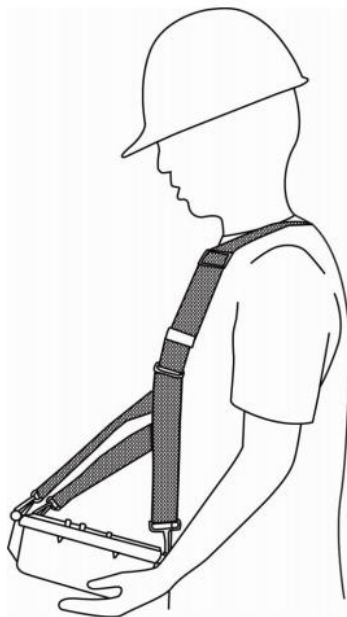


Figure 3.2: Rebarscope Straps

The Rebarscope support straps can be used to hold the Rebarscope once the Rebarscope lid has been removed. When using the Rebarscope support straps, make sure that an eyelet hook is connected to each corner of the Rebarscope as illustrated in Figure 3.2. Two of the hooks clip to the O-rings, while the other two clip around the hinge pins. Based on the Units in use the graphs below in figure 3.3 display the error and accuracy ranges of the rebaroscope in multitude of modes.

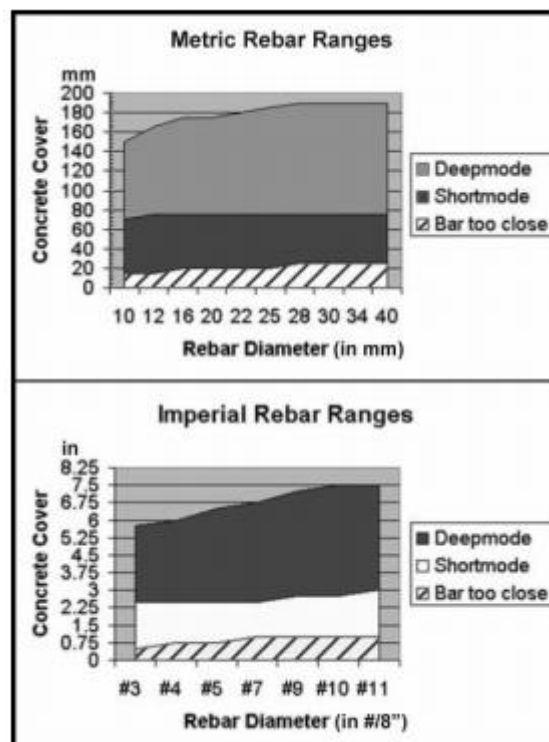


Figure 3.3: Range of Rebarscope

3.3 MODES OF USE AND RESOLUTION

3.3.1 Short Mode. Ideal when reinforcement cover ranges from .5" to 3.0". Locating, determining cover and bar size can all be measured while in this mode. An error of $\pm .125''$ must be accounted for during measurement of metal bar or pipe location.

3.3.2 Deep Mode. Ideal when reinforcement cover ranges from 2.75" to 8". Locating, determining cover and bar size can all be measured while in this mode. An error of $\pm .125''$ must be accounted for during measurement of metal bar or pipe location.

Measurements can often be influenced by proximal rebars especially in parallel arrangement of rebars the neighbouring parallel bar(s). The graph in figure 3.4 shows the minimum spacing to a corresponding resolution.

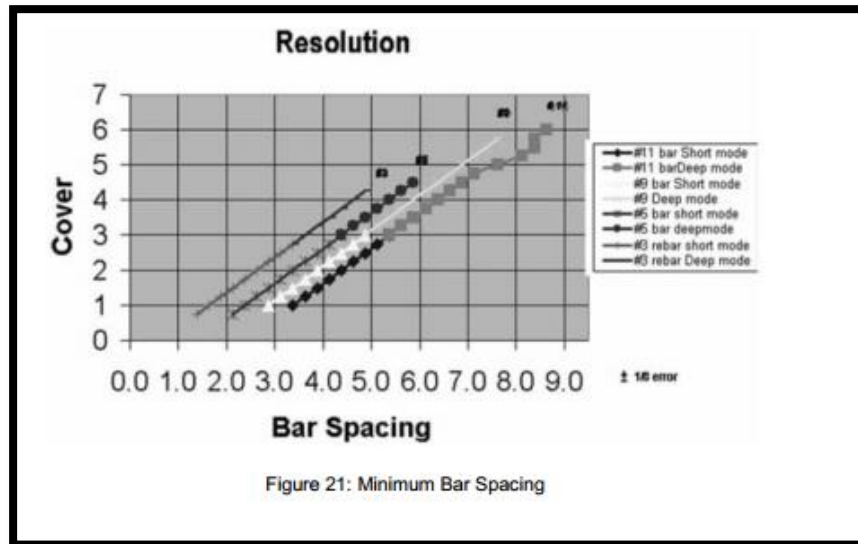


Figure 3.4: Error ranges based on rebar spacing (Rebarscope Manual)

3.4 HANDLING THE REBARSCOPE

3.4.1 Introductory Screen. Attach the sensor probe and the set up the hanging belt along with the Scan cart and the headphones are used as per requirements. Then Switch on the system. The version and time stamp can be viewed as shown in figures 3.5 and 3.6.

- The default screen is the locate cover screen but pressing ESC button shall get you out to the main menu. The main menu has a multiple option as described below
- Locate menu is used for obtaining three types of data:
 - Cover: to evaluate the cover above the rebar.
 - Size: to evaluate the size or the rebar.
 - Statistical spread of cover over the test area.



Figure 3.5: Rebarscope home screen

- The Cover Map menu is used to gather data in the field marking the cover and location of rebars on a 2D-grid.
- The Scan Map Menu is used to mark the cover and location on a surface with the rolling cart.

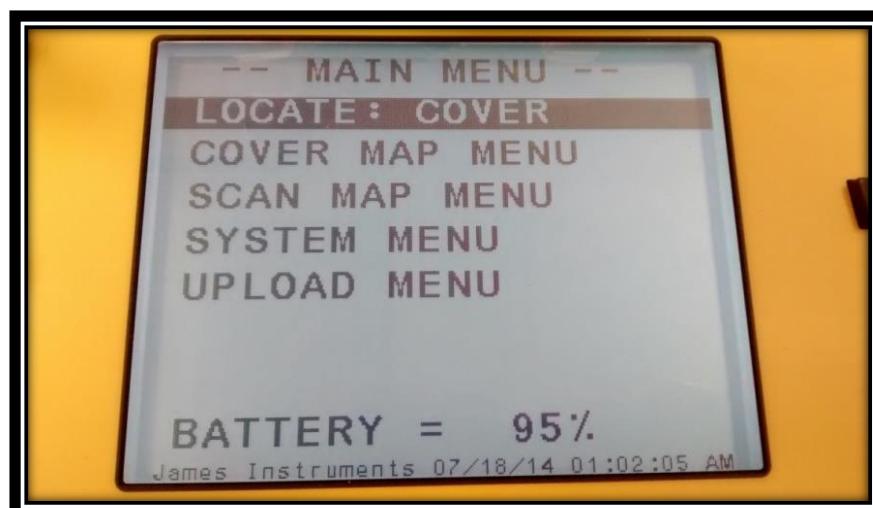


Figure 3.6: Main menu

3.4.2 Evaluation of Rebar Size. The size determination is a 2 step processes: The Figures 3.7 and 3.8 demonstrate the process.

Step 1: Place the sensor(print side on top) on the probing surface, adjust the location of the sensor to maximise the numerical or visual intensity bar and press enter. Using the L shaped template to mark the position.



Figure 3.7: Size screen and sensor



Figure 3.8: Sensor data acquisition

Step 2: Place 3/8” spacer on the surface and place the sensor on it, as shown in figure 3.9. Then press enter to record the intensity of the rebar which would add a known cover of 3/8” of an inch to the recorded data. This should evaluate the bar size embedded within the test surface.

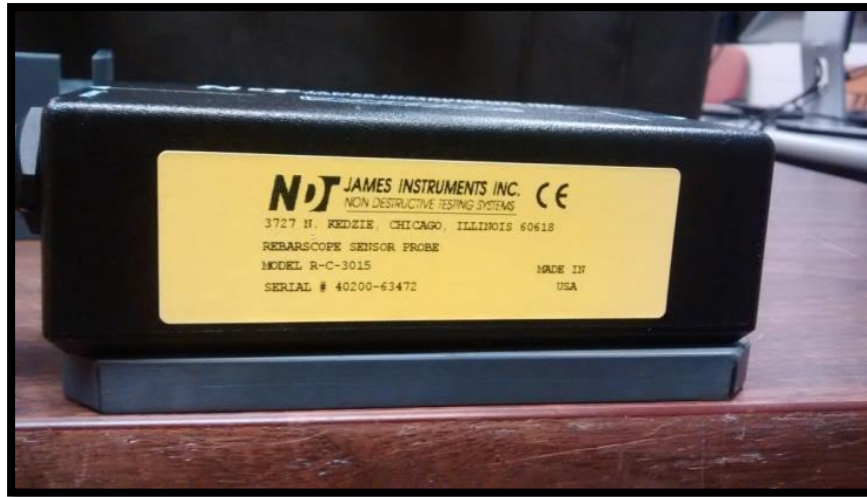


Figure 3.9: Sensor with spacer on surface

- In surfaces where the bar is too near i.e. the numerical value $> 3000(S < 2.0)$, another spacer with thickness $1 \frac{5}{8}$ " is used for both steps (no effect on the evaluation of the bar size). The screen elements follow as shown in figure 3.10

3.4.3 Evaluation of Cover. Material such as concrete between the rebar's and the exposed surface is defined as the cover. The default screen on switching on the instrument is also the locate cover tool.

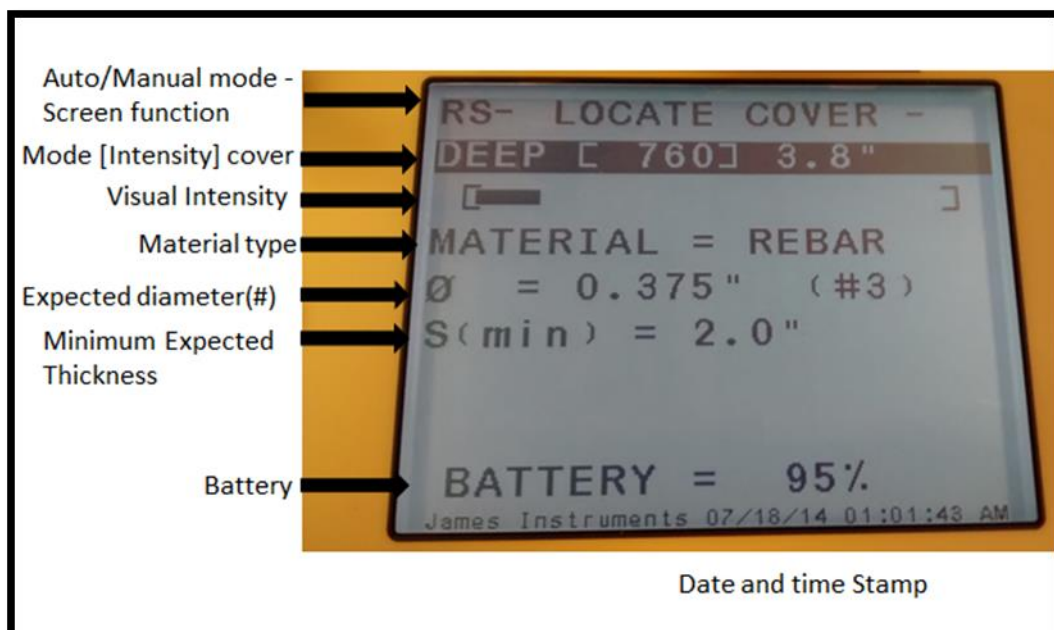


Figure 3.10: Screen elements

- Initially the system is in Automatic mode(RS) which evaluates the approximate cover and chooses the Shallow or deep mode.
- The numerical, visual and audio Intensity parameters can be utilised to locate the precise rebar location. The audio response(3 types) can be activated by pressing the right button when scrolled to visual intensity bar. The left button can be used to toggle between automatic mode and manual mode when scrolled to visual intensity bar.
- The Material can be chosen as per the survey material. Such as:-
- Rebar: metric and imperial reinforcement bars along with post tension cables
- Conduit
- Copper
- The diameter can be determined from and locate size tool and set or chosen from the standard option designated by (#) given by the system, which has influence on the evaluated cover.
- An estimated minimum cover(S_{min}) needs to be chosen for optimum evaluation of cover.

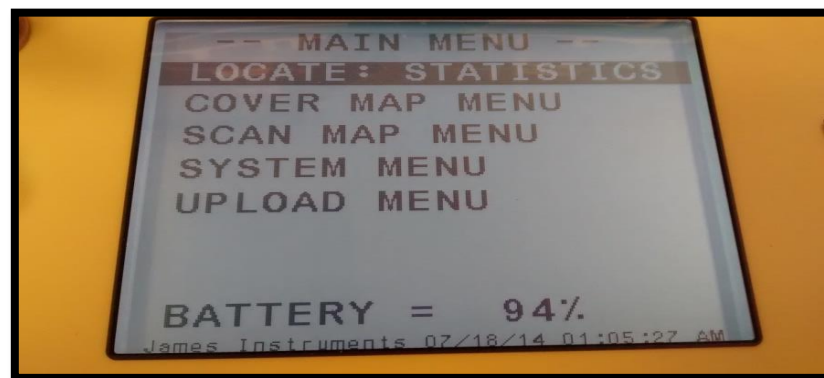


Figure 3.11: Statistical evaluation option

3.4.4 Statistical Evaluation of Cover. This option can be used to compile data to determine statistical average cover during data collection. Also this can be used as a quality testing tool which evaluates and combines the data set of cover values at the test surface, as represented in figure 3.11 and figure 3.12.

Collecting data from each rebar location using the numerical intensity data or pre-marked points on the test surface. The display provides the maximum cover, minimum cover, mean cover and number of samples.

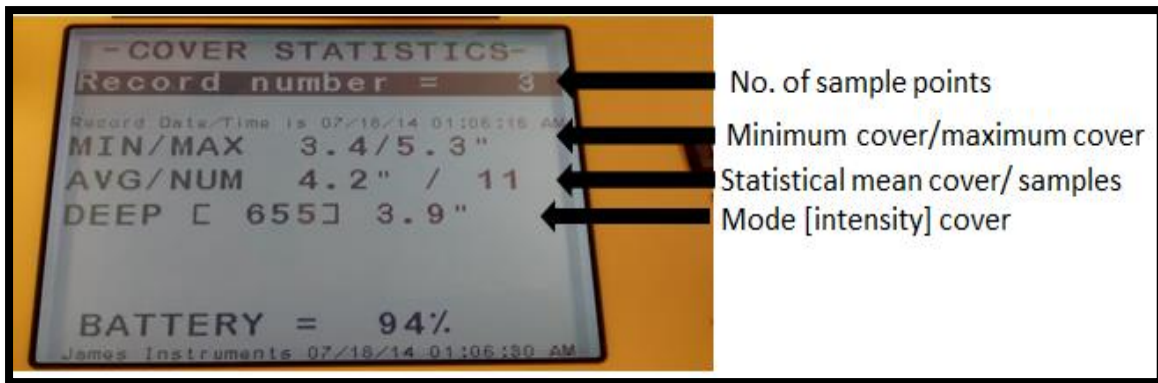


Figure 3.12: Screen for statistical evaluation of the cover data

3.5 COVER MAP MENU

The cover map mode allows the user to mark the cover and location of a rebar on a grid. The grid lines are numerically numbered with the Y axis starting at 1 from left to right. The X axis is also numerically numbered with number 1 starting at the top of the grid. This is illustrated in figure 3.13 below.

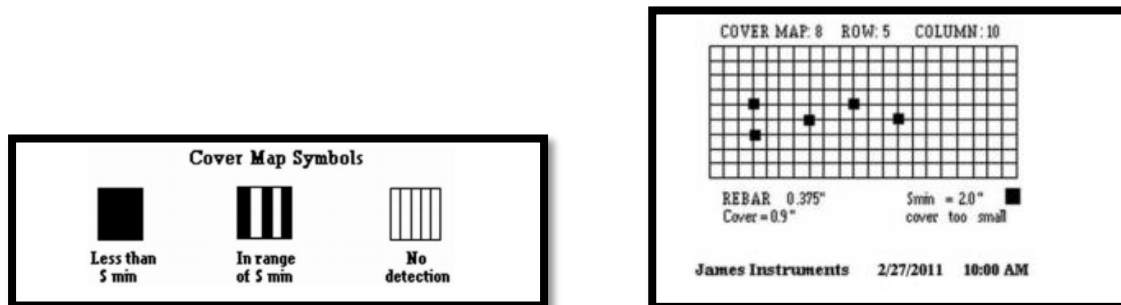


Figure 3.13: Legend for map cover and ranges

The Three symbols below have been selected to allow the user to distinguish the status of the current reading. A full shaded box represents that the cover is less than the selected S_{min} . The S_{min} is the selected minimum cover you have fed into the Rebarscope to detect.

- For each data point on the grid, the rebar size and cover parameters can be noted at the bottom of the grid as shown in figure 3.14. This is the general method best suitable for an area rather than a point data.

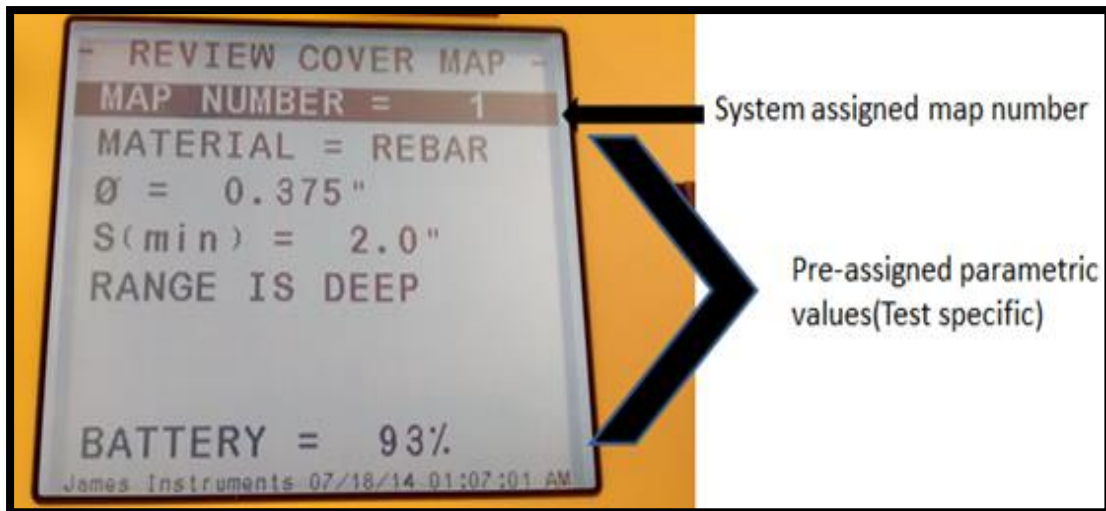


Figure 3.14: Map navigation

- The system assigns Map Number by default and cannot be changed.
- The material of rebar's can be chosen
- The minimum expected cover should be assigned
- The mode of operation i.e. shallow or deep mode should be chosen.

3.6 SCAN MAP MENU

The scan map option allows the user to make use of the scan cart over large surfaces, as illustrated in figure 3.15. The scan cart is ideal for surfaces where the system can acquire data in motion.

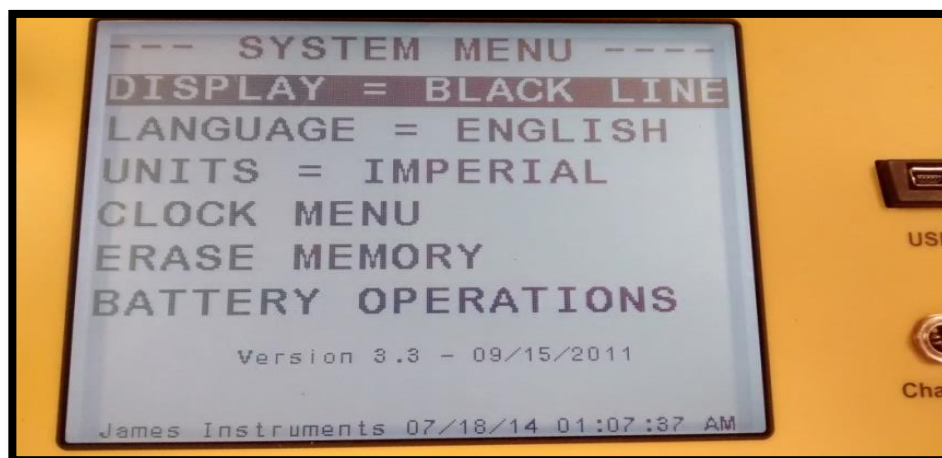


Figure 3.15: System display options

3.7 UPLOAD MENU

The data points from a survey can be uploaded using a USB data cable onto a system to trace 2D map(grid) of location, size of rebar's and the cover. The data can be uploaded in the form of individual records or as cover and scan maps. A com test can be executed to test and verify the optimum working of the system which identifies any anomalies in the connections. Once uploaded the software allows the user to analyse the data, while a graphing tool function allows the creation of a contour map.

4 GROUND PENETRATION RADAR

Unlike traditional radar systems, GPR systems are mainly used to detect and measure the depth of non-homogeneities (either defects or layers) in a dielectric medium. Detection could be achieved by comparing the power of the scattered EM waves produced by the contrast in the dielectric properties between medium and inhomogeneity to a prefixed threshold above the receiver noise level. Depth estimation, however, is more complicated because it requires precise measurement of the time delay between the transmitted signal and the reflected signal. The time delay can then be converted to depth by multiplying it by the speed of EM waves through the studied medium. Original radar systems, working with a CW, did not have this feature because with a CW, it is difficult to set a time marker representing the start of wave transmission and another one representing the reception of the reflections. This problem was overcome in radars and in GPR systems by introduction of modulation of the CW. Depending on the modulation technique used, three types of GPR systems can be identified: the frequency modulated GPR, the synthetic pulse radar, and the amplitude modulated (or impulse) GPR [3] and [4].



Figure 4.1: Ground Penetration Radar system structure scan mini

The StructureScan Mini as illustrated in figure 4.1 is GSSI's all-in-one Ground Penetration Radar system for concrete inspection. This hand held system locates rebar, conduits, post-tension cables, voids and can be used to determine concrete slab thickness in real-time[GSSI website]

The StructureScan Mini safely locates metallic and non-metallic targets within concrete structures up to a depth of 20 inches. The system incorporates an auto target feature that marks the detection of features of interest. This function also estimates the depth of targets and automatically adjusts the depth scale.

The StructureScan Mini is offered in two versions— the original or the StructureScan Mini with 3D. Typical Uses for StructureScan Mini Include:

- Concrete inspection – locate metallic and non-metallic targets in walls, floors and ceilings
- Structure inspection – bridges, monuments, walls, towers, tunnels, balconies, garages, decks
- Condition assessment – map relative concrete condition for rehab planning
- Measure slab thickness
- Void location

4.1 GROUND PENETRATING RADAR TYPES

There are three major types of GPR Systems which are described below.

4.1.1 Frequency Modulated GPR. Frequency modulation of a continuous wave (FM-CW) could be used as a time marker to precisely locate the transmission and reflection events in time. As shown in Figure 34 below, the simplest implementation of this technique is to linearly change the frequency of the CW over time between two limits in a known periodic manner using a voltage controlled oscillator (VCO). The frequency difference, f_d , between the transmitted signal and the reflected signal is proportional to the two-way travel time, t_d , to the inhomogeneity (or target) . The frequency difference is determined by mixing the reflected signal with the transmitted signal via a coherent mixer.

The centre frequency and bandwidth of the transmitted signal from a FM-CW GPR should be suitably selected according to the investigated medium to minimize attenuation and distortion of the reflected signal. Additionally, it is more suitable to use FM-CW GPR systems to detect single shallow in-homogeneities, where the need for a short pulse (or equivalently large bandwidth) to resolve the inhomogeneity is difficult to achieve using the other types of GPR [11]. Multiple inhomogeneity detection, however, is more difficult to accomplish because the difference signal will contain multiple frequency components that need a narrow bandpass filter bank to be resolved, as in figure 4.2.

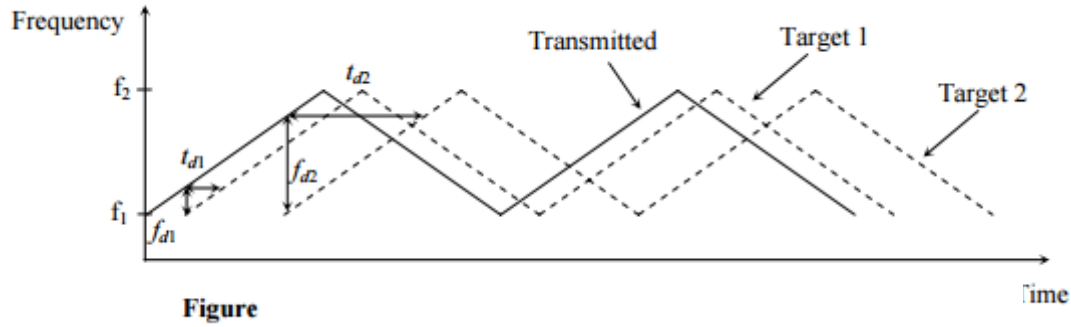


Figure 4.2: GPR signal time frequency diagram

4.1.2 Synthetic Pulse GPR. Synthetic pulse GPR, also called stepped frequency GPR, is similar to the FM-CW GPR where the carrier frequency is modulated. In this design, however, the carrier frequency is varied discretely, rather than continuously, between two frequency limits in N steps. The amplitude and phase of the reflected signals are then precisely measured and recorded for each frequency step, yielding the Fourier Transform (FT) of the reflected signal. A simple inverse fast Fourier Transform (IFFT) can then be applied to the recorded samples to reconstruct the time domain signal from which the detection and range information are extracted. Alternative methods for detection and range estimation can also be applied directly in the frequency domain [5].

4.1.3 Pulsed (or Impulse) GPR. Impulse GPR is the most common GPR system used currently because its data is easier to interpret. An impulse GPR system can be regarded as amplitude-modulated radar, where the transmitted signal is reduced to a very short pulse (in the order of one nanosecond or less) with a wide spectrum (a few GHz). Because of their wide spectrum, impulse GPR systems are referred to as ultra-wide bandwidth (UWB) radars. According to the Federal Communications Commission (FCC), a device is considered UWB if it has a fractional bandwidth greater than 0.25 or if its bandwidth occupies 1.5GHz or more of spectrum when its centre frequency is greater than 6GHz. The fractional bandwidth is defined as $2(f_h - f_l) / (f_h + f_l)$, where f_h and f_l are, respectively, the upper and lower frequencies of the -10dB relative to the maximum emission point, and $(f_h + f_l) / 2$ is commonly known as the centre frequency.

The principle of an impulse GPR system is based on sending a short EM pulse through the antenna to the ground and then recording the reflected pulses from the surface and the internal non homogeneities. The two-way travel time to the targets can then be measured in the

time domain between the reflected pulses. Impulse GPR systems function as follows. A trigger pulse is first generated in the radar control unit. This trigger pulse is then sent to a transceiver where it is modulated and amplified to become a bipolar transmit pulse with a much higher amplitude and bandwidth. The pulse is sent through the transmitting antenna to the ground. After a short time (in the order of few nanoseconds), the reflected signal is collected by the receiving antenna and is then transmitted to the receiver circuitry. It should be noted that the pulse generator produces a large number of pulses at a fixed pulse repetition frequency (PRF). Due to the relatively short range of a GPR system (around 1m [3ft] for pavement assessment), the PRF can be in the order of a few hundred kHz without any ambiguities in range [6]. The resulting reflected signals, which are assumed to be similar because they are collected over the same location, are integrated together in the receiver to produce a single scan with a higher signal to noise ratio (SNR). Because of the wide bandwidth of the received signals, the receiver does not require a super heterodyne architecture like traditional receivers. However, it is usually composed of a low-noise RF amplifier, a wideband bandpass filter to limit the frequency content of the signal, a high-speed sampler, and a high-speed digital-to-analog converter (ADC). Since ADCs cannot work at high sampling frequencies (in the GHz range to meet the Nyquist sampling frequency limit), the entire reflected signal is digitized over a set of identical reflected signals resulting from different trigger pulses, with different samples acquired from each signal. The digitized signal is then transferred to a digital signal processor (DSP), where it is amplified and filtered according to the user-selected parameters. The collected data is finally displayed for immediate interpretation and is stored on magnetic media for later processing.

Due to the pulsed nature of the impulse GPR, it can transmit high peak power EM pulses to ensure an appropriate depth of penetration, with an overall low average power, as in figure 4.3. The transmitted low average power makes impulse GPR systems safer to use than other CW systems[11].

4.2 GROUND PENETRATING RADAR ANTENNAS

Like other systems working with EM waves, a GPR system needs an antenna to transmit and receive EM energy. Depending on the number of antennas used, a GPR system can be monostatic (a single antenna is used for transmit/receive), bi-static (one antenna is used for transmission and another antenna is used for reception), or multi-static (a single antenna or multiple antennas are used as transmitters and multiple antennas are used as receivers). In the case of a monostatic GPR, the transceiver should include a duplexer to protect the receiver from the high power signals during transmission and to direct the low power received signals to the

receiver during reception. Depending on the way antennas are deployed, GPR systems are classified as air-coupled (or launched), or ground-coupled systems.

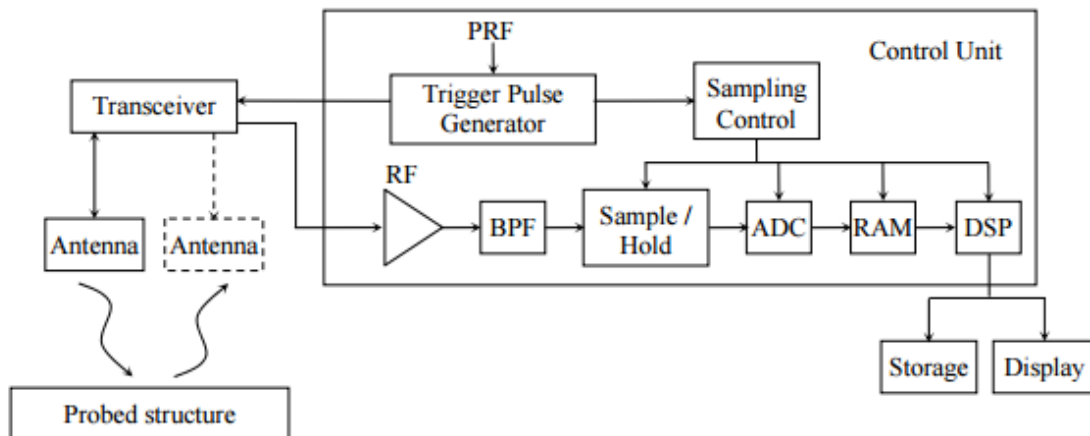


Figure 4.3: Diagram of GPR system processes

In air-coupled systems, the antennas (usually horn antennas) are typically 150 to 500mm above the surface. These systems produce a clean radar signal and allow for highway speed surveys. However, the drawback of these systems is the low depth of penetration into the pavement structure since part of the EM energy, sent by the antenna, is reflected back by the pavement surface. In contrast, a ground-coupled system's antenna is in full contact with the ground, which gives a higher depth of penetration (at the same frequency) but limits the speed of the survey. Ground-coupled antennas are usually in the form of bowtie dipoles.

For easier data interpretation, the GPR antennas are designed to radiate a wave that can be approximated in the far field ($r > 2D^2/\lambda$) by a normal-incidence transverse electromagnetic (TEM) plane wave. This applies also to the case of a bi-static configuration, where the incidence angle is small but different from zero. Moreover, the incident wave is generally linearly polarized. The half power (3dB) beam width varies typically between 20° and 90° .

4.3 ELECTROMAGNETIC THEORY PERTINENT TO GPR SYSTEMS

Electromagnetic wave propagation through a homogeneous medium is governed by Maxwell's equations and the constitutive relations. These equations relate the electric field and the magnetic field at every point to the sources that create them, and to the electrical properties

of the medium. For a source free medium represented by its permittivity, ϵ , conductivity, σ , and permeability, μ , the reduction of Maxwell's coupled equations to a single field equation yields the wave equation. For time-harmonic EM fields with angular frequency ω (assuming time variations of the form $j t e \omega$), the wave equation for the complex electric field $E(\mathbf{r})$ at a spatial point defined by vector \mathbf{r} , is given by equation below.

$$\nabla^2 \mathbf{E}(\mathbf{r}) + \omega^2 \epsilon \mu \left(1 - j \frac{\sigma}{\omega \epsilon}\right) \mathbf{E}(\mathbf{r}) = 0$$

If the electric field is assumed parallel to the x-axis and it depends only on the z coordinate, the second order differential equation can be reduced to:

$$\frac{d^2}{dz^2} E_x(z) + \omega^2 \epsilon \mu \left(1 - j \frac{\sigma}{\omega \epsilon}\right) E_x(z) = 0$$

$$E_x(z) = E_0^+ e^{-jkz} + E_0^- e^{jkz}$$

$$k = \omega \sqrt{\epsilon \mu \left(1 - j \frac{\sigma}{\omega \epsilon}\right)} = \beta - j\alpha, \quad \alpha, \beta \geq 0$$

k is the wavenumber, α is the attenuation constant (Np/m) and β is the phase constant (rad/m). The first term in (2-3) represents a wave traveling in the +z direction, and the second term represents a wave traveling in the -z direction. A time varying representation of the wave traveling in the +z direction is given as follows:

$$E_x(z, t) = \text{Re} \left\{ E_0 e^{-j(\beta - j\alpha)z} e^{j\omega t} \right\} = E_0 e^{-\alpha z} \cos(\omega t - \beta z), \text{ with } z > 0$$

This represents a uniform plane wave since the amplitude and phase of the field at all points in the xy plane at the coordinate z is the same. This wave is exponentially attenuated by a factor α as it propagates in the +z direction. The phase velocity, v , which is, in this case, equal to the energy (or group) velocity, can be obtained by setting the phase of the wave (as a function of time) to a constant and then taking its time derivative:

$$\frac{d}{dt}(\omega t - \beta z) = 0 = \omega - \beta \frac{dz}{dt} \Rightarrow v = \frac{dz}{dt} = \frac{\omega}{\beta}$$

Expressions for α and β as a function of frequency and the constitutive parameters can be derived by squaring equation (2-4), equating its real and imaginary parts, and then solving for α and β simultaneously:

$$\alpha = \omega \sqrt{\mu \epsilon} \sqrt{0.5 \left(\sqrt{1 + \left(\frac{\sigma}{\omega \epsilon} \right)^2} - 1 \right)}$$

$$\beta = \omega \sqrt{\mu \epsilon} \sqrt{0.5 \left(\sqrt{1 + \left(\frac{\sigma}{\omega \epsilon} \right)^2} + 1 \right)}$$

For a good dielectric material at a high frequency, such as a pavement material probed by GPR at 1GHz nominal frequency, the quantity $(\sigma/\omega\epsilon)^2$ is usually small compared to 1. Moreover, due to the non-magnetic nature of the pavement materials, the permeability μ can be approximated by the permeability of free space μ_0 . Therefore, approximate expressions for α , β and v can be derived according to the following equations:

$$\alpha = \frac{\sigma}{2} \frac{\eta_0}{\sqrt{\epsilon_r}}$$

$$\beta = \frac{\omega}{c} \sqrt{\epsilon_r}$$

$$v = \frac{c}{\sqrt{\epsilon_r}}$$

where:

- η_0 : wave impedance of free space, $\eta_0 = \sqrt{\frac{\mu_0}{\epsilon_0}} \approx 120\pi \Omega$
- ϵ_r : relative permittivity or dielectric constant of the medium
- c : speed of light in free space, $c = \frac{1}{\sqrt{\epsilon_0 \mu_0}} \approx 3 \times 10^8 \text{ m/s}$

It should be noted that the dielectric constant, ϵ_r , is usually complex, with the real part representing energy storage in the media and the imaginary part representing loss due to dielectric effects. To account for that loss, the imaginary part of ϵ_r should be incorporated into the attenuation factor α . However, because conduction loss is usually much higher than dielectric effects loss, the dielectric constant can be considered as a real number, provided that conduction loss is accounted for, as specified by the equation .Moreover, for many materials, the dielectric constant of a medium depends on the frequency of the EM waves[11]. Consequently, signal components of different frequencies will travel with different speeds, which results in the distortion of the signal (dispersive media). Nevertheless, the dielectric constant of concrete bridge materials does not vary significantly in the GPR bandwidth (For dried concrete ϵ_r varies between 4 and 12 and σ varies between 0.003S/m and 0.009S/m, for 9% saturated concrete, ϵ_r varies between 8.5 and 7.5 and σ varies between 0.06S/m and 0.14S/m ([7] and [8]) in the frequency band 0.5GHz to 1.5GHz. Other authors reported higher values depending on the mixes used [9]). Hence, ϵ_r can be considered as a constant (versus frequency) [10] to facilitate data interpretation.

5 DATA ACQUISITION AND PROCESSING

The Rebarscope and the Ground Penetration System both are easy to operate and the process of data acquisition is fast. The concrete slabs were both marked with a square grid to standardise the data acquisition process. The data acquisition was performed multiple times and stacked to obtain average values.

5.1 GROUND PENETRATING RADAR INVESTIGATIONS

The Ground penetration radar data is acquired along a traverse as explained earlier. Its records reflection from any surface where there is change in dielectric permittivity. Based on the known design of the concrete slabs a 6 inch spaced grid was carefully designed so as to acquire the data in the optimised technique. Predominant parameters were taken into consideration such as spacing of the rebars, the depth, etc. GPR data were collected using high frequency antennas (2.6GHz), manufactured by GSSI, as in figure 5.1, which provided high-quality data with great lateral and vertical resolution for assessing the integrity of the reinforced concrete structures and their conditions. The GPR signal's reflection, its attenuation from the top layer of the reinforcing steel in the transverse direction, was captured. The GPR units were properly calibrated for each concrete slab to obtain accurate distance measurements.



Figure 5.1: GPR data acquisition

The appropriate acquisition and processing parameters were developed individually for both concrete slabs in order to conduct a rapid, efficient assessment. Data was acquired multiple times across similarly placed traverses for a spatial comparison and to address statistical

calibration of the data. In order to follow the established procedure and make further data analysis easier, the Concrete and its dielectric constant were assumed uniform during the GPR data acquisition.

For the purposes of the depth control in one slab, dielectric constant was individually adjusted at multiple values to ascertain any variations in the results over the same traverse. The acquired data, as in figure 5.2 were sorted and processed using GSSI RADAN 7 software for normalization and numerical analysis. The relative coordinates, arrival times (nanoseconds, ns) and amplitudes (normalized decibels, NdB) of the reflections from each imaged segment of transverse reinforcement steel were captured in a Microsoft Excel spreadsheet. The travel times of the GPR signal were converted into apparent depths.



Figure 5.2: Data acquisition

The reflection amplitude distribution was carefully observed analysed and segregated to distinguish emerging patterns, based on the depth correlation and any other factors. The amplitude loss, due to deliberately placed obstructions was also observed.

5.2 REBARSCOPE

As done to acquire the GPR data the same square grid was used to acquire the Rebarscope data. The Rebarscope data, as in Figure 5.3 varies from the GPR data in the manner

that Rebarscope provides a point data rather than a traverse like the GPR. Based on the known design of the concrete slabs a half inch 6 inch spaced grid was used to acquire the data.



Figure 5.3: Rebarscope data acquisition

Predominantly data is recorded on a grid map with data points vertically above the rebar locations. As the instrument shows highest intensity vertically above the rebar section thus zeroing in on the rebar location. Based on the signal response the intensity of signal may vary.

The induction current technology isn't affected by presence of any conductive particulates in the cement but is only effected by big conductive material like rebars, one important limitation which we are not studying here would be close clusters of rebars which could make the rebar distinguishing ambiguous, some dominant parameters were taken into consideration such as spacing of the rebar material as conductivity would vary for different material, the depth which is needed to input for a minimum cover value.

Rebarscope data is collected using high James Instruments product which is among the best available in the market, which provided high-quality data with great vertical depth resolution and the approximate rebar thickness, for assessing the accurate depth of the rebars. The Rebarscope signa, as in figure 5.4 reflection and its intensity of the reinforcing steel was captured. In cases of dense rebars or multiple conductive particulates presence the Rebarscope should also be calibrated with ground truthing.



Figure 5.4: Data acquisition of slab 1 with variable depth

Separate grid maps are used for both the concrete slab units. The appropriate acquisition and processing parameters were developed individually for both concrete slabs in order to conduct a rapid, efficient assessment. The slab 1 with multiple depths of rebars was operated under shallow and deep mode both to compare them, automatic mode is best as it instantly calibrates as per approximate signal based on the rebar depth values. Data was acquired multiple times across similarly placed points to address statistical calibration of the data. In order to follow the established procedure and make further data analysis easier, the Concrete was assumed uniform during the data acquisition. The acquired data was sorted and maps were uploaded with data onto computer and a grid based data was made for ease of understanding. Microsoft Excel sheet were developed with the Cartesian coordinates and the rebar depth at that location.

The Rebarscope data in general could be little erroneous in nature if the proximal rebars are close by as shown in its error ranges plot. To overcome the proximity errors and minimise the systems intrinsic errors we took data directly on the slab and also with a small flat plastic piece with known width. Then a method was developed to eliminate the errors which are discussed in the Analysis part. To obtain understanding of any temperature effects, the GPR data and the

Rebarscope data was acquired once after snow and once after rain to see any effects on the data obtained.

5.3 DATA PROCESSING AND ANALYSIS

In Radan 7 and the in a simplistic manner the processing involves the following steps:

- After opening the .DZT file, do a zero correction to remove the air zone above the concrete.
- Interactive mode needs to be activated
- From the tools ‘ground truth’ tool has to be chosen to estimate optimum dielectric Permittivity value.
- Then choose the single point option and mark up just below the hyperbolas as marked up in the illustration.
- These points shall show the parameters associated with them such a two way travel time and Amplitude values.

The above steps are very primitive in nature which doesn't involve any filters or migration or de-convolution of the data which are employed to improve the quality of the data. But as in the data, as in figure 5.5; we see here is of quite good quality to work with and doesn't need much complex processing steps. The figure 5.6 shows the grid data from Rebarscope which explains a mathematical correction to the Rebarscope data which needs no processing typically.

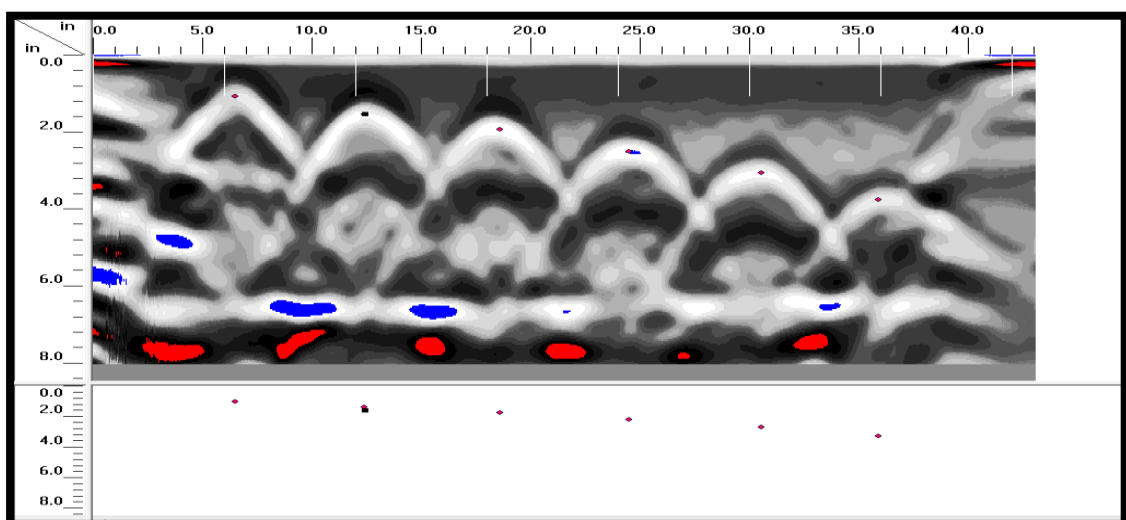


Figure 5.5: Ground Penetration Radar data

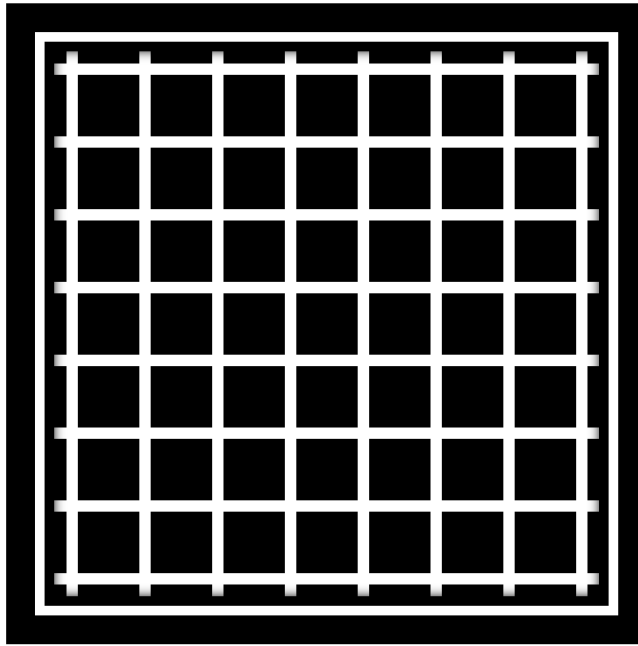


Figure 5.6: Rebarscope map with data points

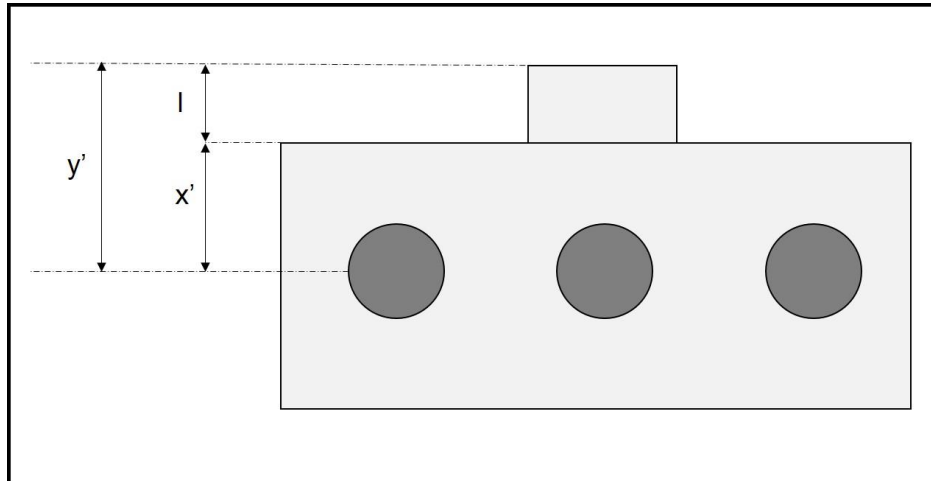


Figure 5.7: Model of slab and depth parameters

X = real depth of rebar from the surface of the concrete

y = real depth of rebar from above the object

x' = apparent depth from top of concrete from rebaroscope

y' = apparent depth from top of object from rebaroscope

$$\begin{aligned}
 x' &= x - 2\Delta d \\
 y' &= y - 2\Delta d \\
 y' - x' &= y - x
 \end{aligned}$$

Here we had eliminated any Δd caused by rebars in proximity or any other objects causing error.

$$\frac{y - x}{l} = \frac{x'}{x} = \frac{y'}{y}$$

Here, we calibrate the ratio based intrinsic error caused by the instrument. Thus, eliminating majority of systematic errors caused in the Rebarscope data.

5.4 ANALYSIS (PARAMETERS)

5.4.1 Location. This is an indirect parameter inferred from the GPR based on survey wheel calibration and the predesigned survey grid, as for the Rebarscope it's obtained on the grid in the location with highest intensity of induction current . The ground Penetration Radar system is very accurate with the X-Y plane location of the rebars. The errors associated with the Cartesian locations in the X-Y plane are minimal and their range is +- 0.05 inch. The Rebarscope intensity bar goes up when it is right above a conductor like rebar, and it's precision is also within +- 0.1 inches based on the sensors size.

5.4.2 Two-way Travel Time. The Signal from GPR is released and then captured and the travel time for the signal is recorded which is a direct parameter obtain in the GPR data analysis. The two-way travel time is influenced by the mediums between the Signal source/receiver and the reflective surface. This involves, the air medium and in this case the concrete and as we consider reflection from the top of rebars, we don't expect any other mediums interference (not considering any defects). In the Radan7 software the reinforcing rebars are picked based on the hyperbola peaks, the two-way travel times for each pick are obtained. The tables below, table 5.1 and figure 5.8 represent the two-way travel times for both the slabs respectively. As the EM wave velocities are very high the two way travel times are measured in nanoseconds.

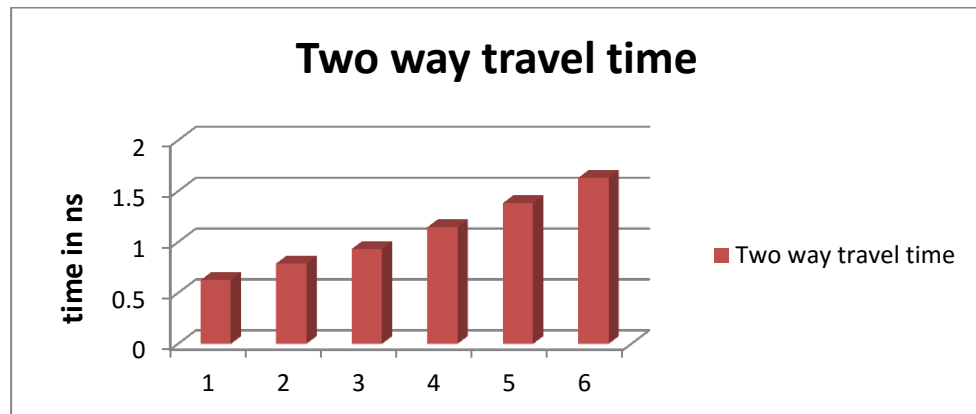


Figure 5.8: Two way travel times for Slab 1

Table 5.1: Slab 1 two way travel time

Rebar Number	Avg. Two-way Travel time (traverse 1)	Difference In time	Avg. Two-way Travel time (traverse 2)	Difference In time	Avg. Two-way Travel time (traverse 3)	Difference In time
1	0.64		0.62		0.62	
2	0.79	0.15	0.79	0.17	0.79	0.17
3	0.95	0.16	0.93	0.14	0.92	0.13
4	1.15	0.2	1.15	0.22	1.14	0.22
5	1.42	0.27	1.37	0.22	1.36	0.22
6	1.64	0.22	1.64	0.27	1.62	0.26

As it can be observed from the graph the two-way travel time increases with consecutive rebars, which is consistent with the known information that the consecutive rebars are placed half an inch below the other. The two-way travel time's error range is by up to ± 0.06 ns seconds which would be ± 0.03 ns for one way travel time. This will manifest into an error less than ± 0.1 inch in the depth values of the rebar which is permissible for most engineering studies.

The Slab 2 as known has rebars placed at a consistent depth. But some of the rebars have obstacles in them. This can be observed in the increased two way travel time of the signal, as illustrated in figure 5.9 and table 5.2.

Among the regions with no obstacles it can be observed that the two way travel time has an error range of less than ± 0.1 ns which would manifest as ± 0.05 ns for on way travel time which results in a error range of ± 0.2 in the apparent velocity of the material.

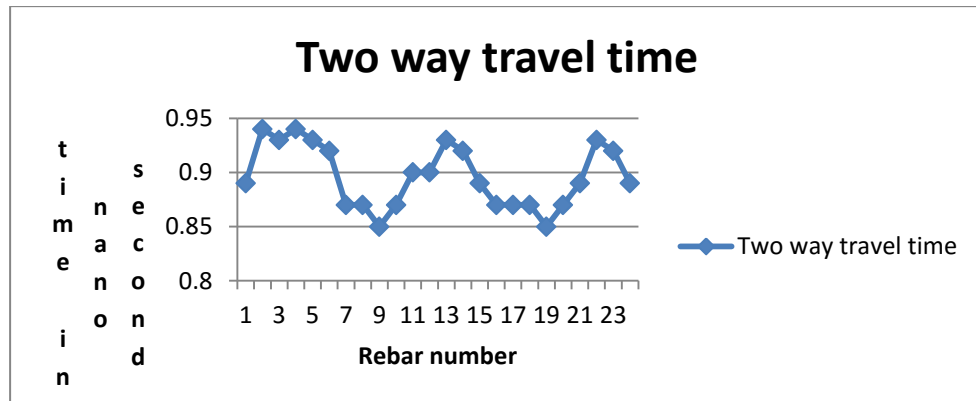


Figure 5.9: Two way travel time for Slab-2

Table 5.2: Slab 2 Two way travel time for rebar reflections

Rebar number	Avg. two-way travel time (traverse 1)	Avg. two-way travel time (traverse 2)	Avg. two-way travel time (traverse 3)	Y- coordinate inches
1	0.90	0.87	0.87	6
2	0.89	0.87	0.87	12
3	0.87	0.85	0.87	18
4	0.89	0.87	0.85	24
5	0.94	0.9	0.87	30
6	0.93	0.9	0.89	36
7	0.94	0.93	0.93	42
8	0.93	0.92	0.92	48
9	0.92	0.89	0.89	54

The Slab 3 as known has rebars placed at a consistent depth. But some of the rebars have obstacles in them, to generate defects in concrete. This decrease in the two way travel time as the defects placed have dielectric permittivity values lower than that of concrete. It can be observed in the decreased two way travel time of the signal in certain zones, as in table 5.3.

Table 5.3: Slab 3 Two way travel time for the rebar reflections

Rebar Number	Avg. two-way Travel time (Traverse 1)	Avg. two-way Travel time (Traverse 2)	Avg. two-way Travel time (Traverse 3)	Y-coordinate inches
1	1.04	1.01	1	6
2	0.88	1	1	12
3	0.89	0.98	1	18
4	1.03	1	0.98	24
5	1.09	1.04	1.01	30
6	1.07	1.04	1.03	36
7	1.09	1.07	1.07	42
8	0.82	1.06	1.06	48
9	0.84	1.03	1.03	54

Dielectric for slab 2 is 6.62 and slab 3 is 8.77

The two way travel times are elevated in zones of the concrete where defects were placed. These are expected. The dielectric constant of a card board is 3as for paper so should be around that so less than concrete so signal should be faster.

5.4.3 Depth (Apparent and Real). This would rather be prime parameter to be obtained in a Ground Penetration Radar survey and that of a Rebarscope. From the rebaroscope it is a directly obtained parameter, whereas for the Ground Penetration Radar System it is a indirectly obtained parameter, as shown in table 5.4, they are compared in table 5.5 and figure 5.10.

From the Rebarscope data the average depths obtained all the Rebars is as following:

Table 5.4: Slab 1 rebar depths

SLAB - 1	Rebar 1	Rebar 2	Rebar 3	Rebar 4	Rebar 5	Rebar 6
Real Depth	1.0in	1.5in	2.0in	2.5in	3.0in	3.5in
Avg. Estimated Depth From Rebarscope	0.98in	1.46in	2.03in	2.52in	2.99in	3.55in
Avg. Estimated Depth From Rebarscope	1.21in	1.61in	1.94in	2.45in	2.97in	3.3in

Depth in inches

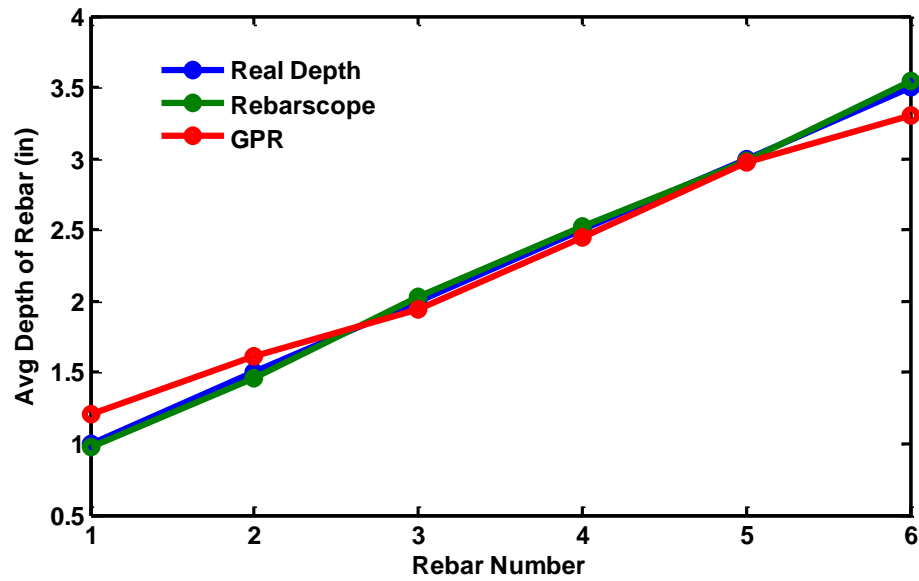


Figure 5.10: Estimated depth of rebar

Table 5.5: Depth values comparative

Rebar Number	Avg. depth Of rebar(in) (GPR)	Avg. depth Of rebar(in) (Rebarscope)
1	1.87	1.87
2	1.849222	1.86
3	1.807667	1.84
4	1.849222	1.85
5	1.953111	1.89
6	1.933333	1.90
7	1.953111	1.88
8	1.932333	1.88
9	1.911556	1.87

For the Slab 2 which has pristine concrete without any defects illustrate the error ranges. These error ranges put's our assumption of concrete homogeneity to test. From the plot below it

can be observed that the ± 0.15 inches, as in figure 5.11. The depths are all compared in figure 5.12 and the error ranges can be observed.

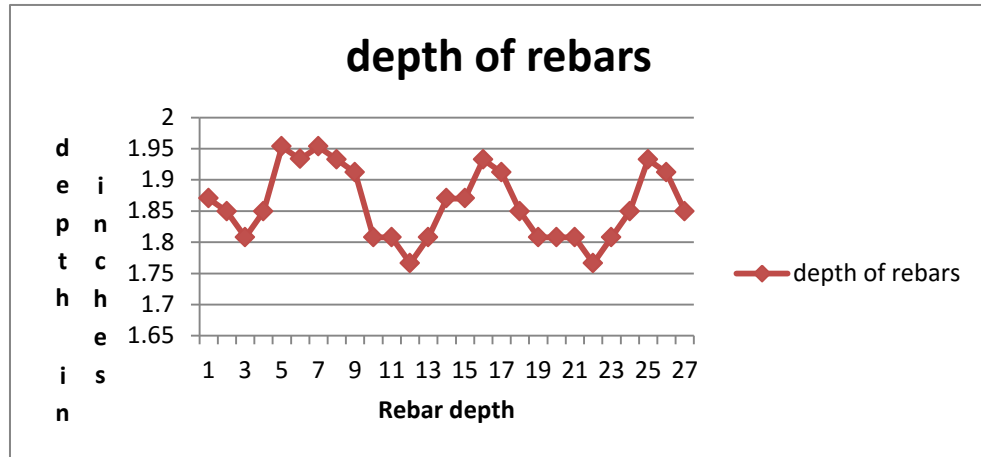


Figure 5.11: Depth of rebars for Slab 2

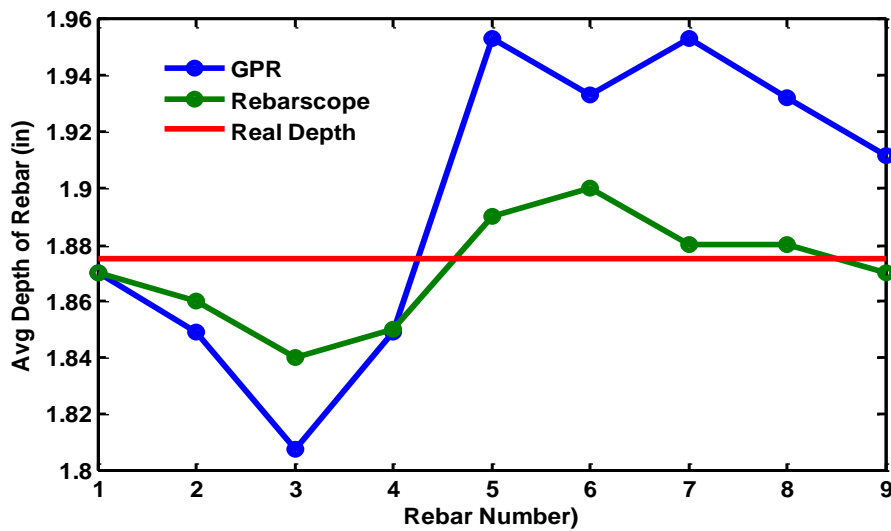


Figure 5.12: Slab-2 depth plots

The Slab 3 has placed cardboard pieces in certain zones and from the table 5.6 it can be observed that the apparent depths of rebars are lower than the real depths. The data observed is consistent with the placed defects. The dielectric permittivity of paper and its products is 3. Thus, reducing the overall two way travel time. The rebarscope estimates the depth with higher accuracy and help overcome the ambiguity; this can be observed in figure 5.13.

Table 5.6: Slab 3 rebar depths

Rebar Number	Avg. depth of rebar (GPR)	Avg..depth of rebar (Rebarscope)
1	1.884	1.87
2	1.595	1.86
3	1.619	1.84
4	1.866	1.85
5	1.975	1.89
6	1.939	1.90
7	1.975	1.93
8	1.488	1.86
9	1.525	1.88

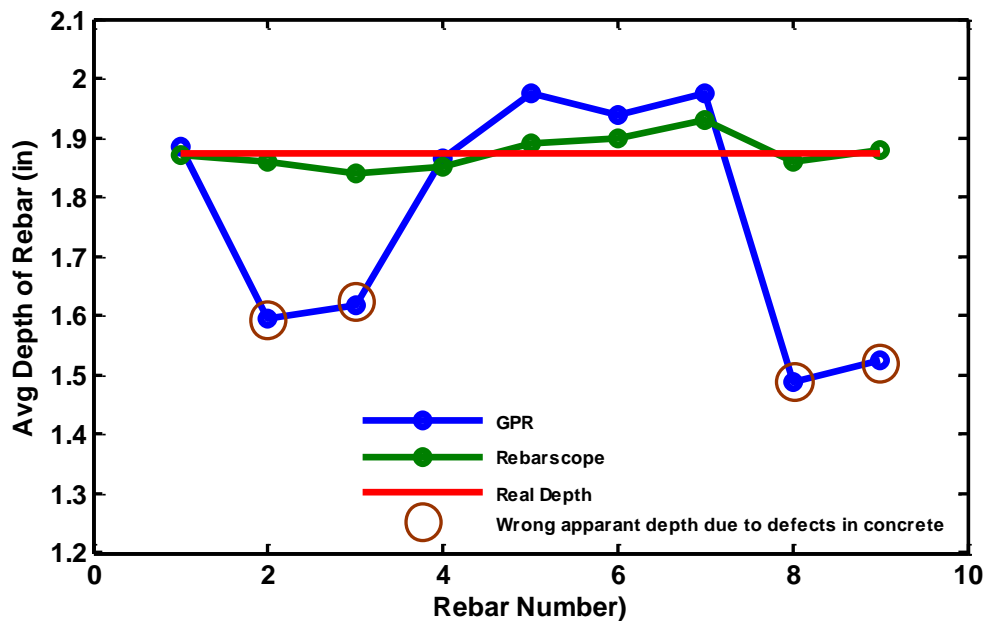


Figure 5.13: Slab 3 rebar depth estimated and real values

As we can observe the Rebarscope data is accurate to the range of ± 0.1 inches which in comparison with variations caused by the small variation in the dielectric permittivity values is very low and wouldn't cause false variation in the dielectric permittivity, as shown in figure 5.13. Though an important observation made in data acquisition is the variation of intensity scale observed in the rebaroscope based on the length of the rebars, also presence of other conductors can cause errors in the data. A specific case could be presence of metal based wiring of the

rebars at junctions of overlapping and overlapping rebar are problematic in rebar depth estimates as they tend to act as a single conductor and represent erroneous depth of the rebar.

The Ground Penetration rebar depth data which is obtained from two way travel time and the estimated Dielectric Permittivity formulae as shown below.

5.4.4 Dielectric Permittivity. The Physical property that influences the velocity of the Electromagnetic waves in a medium is the Dielectric Permittivity. As we assume the concrete to be homogeneous we expect the dielectric permittivity to be a constant. This assumption is a contradiction in itself as any deteriorated region of concrete has a different value of dielectric permittivity which is partially the objective of a GPR study, to observe variations in the dielectric permittivity. During Survey the DP is assumed to be between 5-8 based on the age of the concrete as proposed(Sasha Paper). But during processing based on Ground truth calibration is done. Here as the concrete slabs has rebars all at known depth. Multiple sets of ground calibration was performed and the Dielectric Permittivity values were found as shown in the table 5.7.

Table 5.7: Dielectric permittivity's estimated for the three slabs

Slab 1	Slab 2	Slab 3
5.77	6.62	8.77

The variation in the Dielectric Permittivity values result due to intrinsic defects in the concrete and during construction, as theoretically the concrete is not homogeneous in nature. The two value which are outliers are observations near the rebars where deliberate defects were placed. This is merely to demonstrate the erroneous estimation of dielectric permittivity of the concrete even in cases of good depth understanding of the rebars. Such a scenario is very much plausible in real world scenario, where the ground truth values can mislead the survey and analysis process.

An important observation to make is that the Dielectric Permittivity of the three slabs varies even though they were all constructed at the same time. This can be attributed to the environment they were put in. The slab 1 was placed outdoor with direct sunlight exposure whereas the Slab 2 was placed indoor majority of the time. Thee Slab 3 was moved outdoors after being kept indoors for a few weeks. This does elevate a trend of decrease in dielectric Permittivity with direct exposure to sun and outdoor environment.

5.4.5 Amplitude. The Amplitude loss of the Electromagnetic signals is a very elegant parameter as it can qualitatively indicate relative change in dielectric permittivity more specifically suitable to our study it indicates quantitative degradation of concrete in any form, as most of the form of degradation in concrete tend increase moisture content, chlorides and other chemical components as represented in figure 5.14. These tend to have a higher dielectric permittivity which causes increase in two way travel time and relevantly cause an increased loss in amplitude in relation to a pristine concrete. So a relative comparison in the loss of Amplitude is a good qualitative indicator of degradation of the concrete.

The Amplitude is evaluated in terms of Normalized dBel units, which is dimensionless unit of the logarithmic factor of increase or decrease in signal amount. Aleksey Khamzin part of his doctoral thesis has established values of Amplitude loss categorising them, as shown in figure 5.15 into good and permissible concrete to a cut off value of amplitude loss below which the concrete is degraded to the extent when it needs to be replaced.(Shown in figure below).

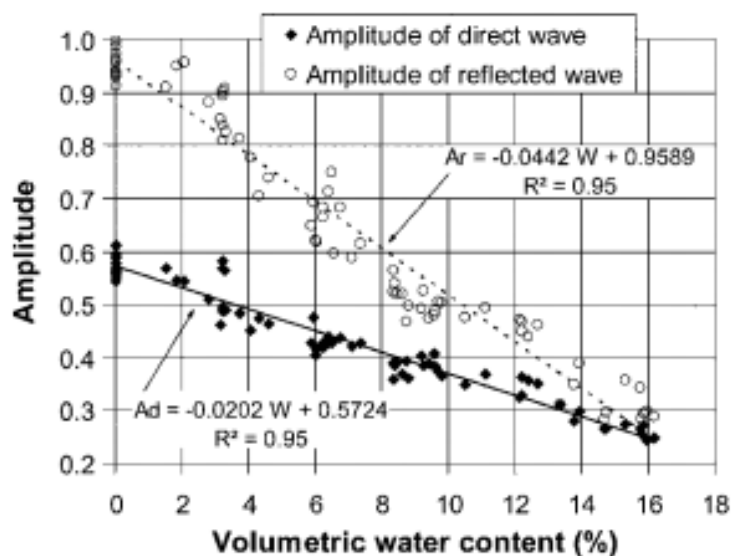


Figure 5.14: Amplitude and moisture contents relationship

Effect of Concrete Moisture on Radar Signal Amplitude by Zoubir Mehdi Sbartai, Stéphane Laurens, Jean-Paul Balayssac, Gérard Ballivy, and Ginette Arliguie (Dec, 2006)[6]

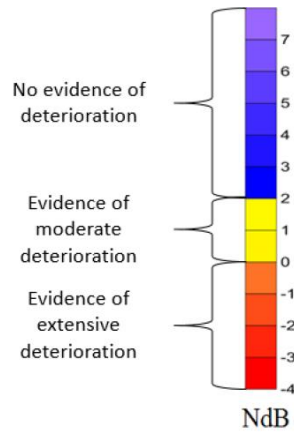


Figure 5.15: Amplitude vs deterioration relationship

He used a different Ground Penetration System and the amplitude values can be calibrated and in the Table below it can be observed Amplitude data from the Slabs with the modified calibrated values. Based on the predesigns of the concrete slabs.

The amplitude based categorization of concrete condition is very valuable but when dealing with deteriorated bridge deck. A plain horizontal surface is not the case and from the illustrated graph below from [5]. The small angle changes cause high error ranges in the received signal Amplitude, as shown below in figure 5.16. So to rely on signal amplitude could lead to inconclusive results in cases. To avoid it would be recommendable to corroborate the amplitude results with better dielectric permittivity results.

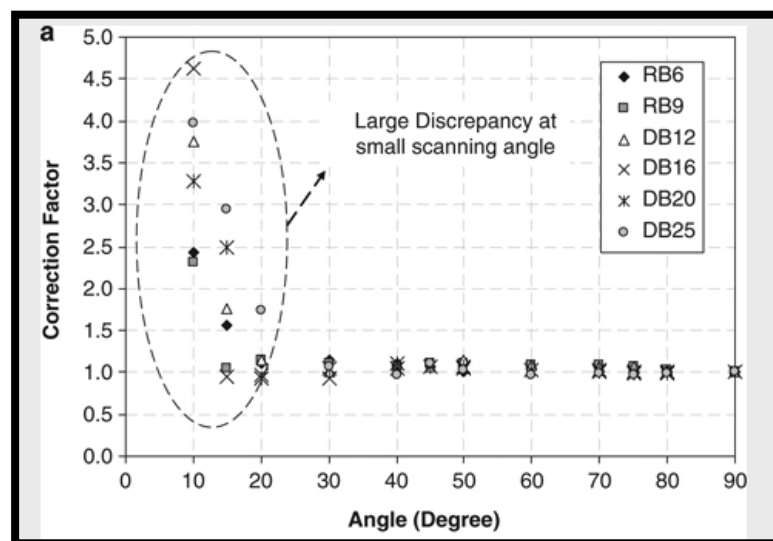


Figure 5.16: Sensor angle vs correction factor

One important element to note would we take into consideration the variation caused by external factors of weather effecting the temperature which would manifest as variations in the Dielectric Permittivity and the Amplitudes. This has been very well represented in [3] where the authors collect data in varied time and note slight variation in the resultant parameters.

6 CONCLUSION

The fundamental question with which the Project began was get a good understanding of the GPR parameters and Rebarscope Parameters and use them in combination to better estimate the differential quality of the concrete. This would improve our protocols of Bridge deck assessments. Some salient set of conclusions for the comparative study are:

- Ground Penetration Radar system is intrinsically a superior tool for non-destructive survey of reinforced concrete over Rebarscope technology. It provides a quantitative estimation of rebar depth and Amplitude loss both of which are indicative of the concrete quality. One major limitation of the GPR study though is construction defects which can be corrected for by a Rebarscope study.
- Rebarscopes have a limitation where presence of proximal rebars or any other conductors could cause estimation of a pseudo depth value of a rebar, to address this limitation a procedure was developed to eliminate systematic errors in depth estimation, which when executed significantly overcome some of the limitations of the Rebarscope thus reducing the errors in the depth measurements of the rebars.
- In degraded concrete a purely GPR study has a scope of ambiguous data, but when GPR study is assisted by a Rebarscope study, depth estimation results tend to be significantly accurate to isolate and map the delaminated and degraded concrete.
- The study of Slab 1 highlighted that there is no considerable variations in the amplitude of the GPR signal with depth variations of the rebars. Also, that the error tend to elevate with depth increment of the rebars.
- The study of Slab 2 and Slab 3 provided error ranges for two-way travel time and apparent depth estimations.
- GPR surveys of reinforced concrete assume the concrete to be homogeneous and this study indicates that within an error range of ± 0.2 inches this assumption is valid.

This study would be step forward in using non-destructive geophysical techniques in concrete based structures like bridges, tunnels and refurbishment of old constructions. From prior reports which tend to utilize the amplitude of the Electromagnetic signal as an indicator or the deterioration, which is reliable in majority of cases but could be ambiguous in some case scenarios, accurate depth estimates shall provide with better estimates of dielectric permittivity, which shall also be reliable indicators of grade of deterioration of concrete. This is a very convenient and vital step forward in Non-destructive Geophysical techniques specifically dealing with reinforced concrete structures, with construction errors.

BIBLIOGRAPHY

- [1] Varnavina, Aleksandra V., et al. "Data acquisition and processing parameters for concrete bridge deck condition assessment using ground-coupled ground penetrating radar: Some considerations." *Journal of Applied Geophysics* 114 (2015): 123-133.
- [2] Portland Cement Association (PCA), 2013. "Corrosion of embedded metals." Portland Cement Association, <http://www.cement.org/tech/cct_dur_corrosion.asp> November 2013.
- [3] Varnavina, Aleksandra V., et al. "Concrete bridge deck assessment: Relationship between GPR data and concrete removal depth measurements collected after hydrodemolition." *Construction and Building Materials* 99 (2015): 26-38.
- [4] Smith, J., Virmani, Y., 2000. "Materials and methods of corrosion control of reinforced and prestressed concrete structures in new construction." Report, Federal Highway Administration, FHWA-RD-00-081, November 2013.
- [5] Sahamitmongkol, Raktipong. "Effect of scanning direction on amplitude of reflected pulse radar from steel bar." *Journal of Building Appraisal* 6, no. 1 (2010): 21-33.
- [6] Sbartaï, Zoubir Mehdi, Stephane Laurens, Jean-Paul Balayssac, Gerard Ballivy, and Ginette Arliguie. "Effect of concrete moisture on radar signal amplitude." *ACI materials journal* 103, no. 6 (2006): 419.
- [7] Missouri Department of Transportation (MoDOT), 2013. "Engineering polity guide." Design Guide, Section 751.10.1.5, Missouri Department of Transportation. Jefferson City, MO, October 2013.
- [8] Vu, K., Stewart, M., (2000). "Structural reliability of concrete bridges including improved chloride-induced corrosion models." Journal Article, *Structural Safety* 22, pp. 313-333, October 2013.
- [9] Thomas, M.D.A., Fournier, B., Folliard, K.J., (2013). "Alkali-aggregate reactivity (AAR) facts book." Report, Federal Highway Administration, FHWA-HIF-13-019, November 2013.
- [10] Al-Khaja, W., (1997). "Influence of temperature, cement type and level of concrete consolidation on chloride ingress in conventional and high-strength concretes." Journal Article, *Construction and Building Materials*, Vol. 11, No. 1, pp. 9-13, November 2013. 130.
- [11] Lahouar, Samer. "Development of data analysis algorithms for interpretation of ground penetrating radar data." PhD diss., Virginia Polytechnic Institute and State University, 2003. [12] Zemajtic, J., (2013).

- [12] “Curing concrete in construction.” Portland Cement Association, <http://www.cement.org/tech/cct_curing.asp> November 2013.
- [13] Kan, L., Shi, H., Sakulich, A., Li, Vi., (2010). “Self-healing characterization of engineered cementitious composite materials.” Journal Article, ACI Materials Journal, Vol. 107, No. 6, pp. 617-624, November 2013.
- [14] Sakulich, A., Bentz, D., (2011). “Increasing the service life of bridge decks by incorporating phase change materials to reduce freeze/thaw cycles.” Journal Article, Journal of Materials in Civil Engineering, Vol. 24, No. 8, pp 1034-1042, November 2013.
- [15] Gucunski, N., Romero, F., Kruschwitz, S., Feldmann, R., Parvardeh, H., (2011). “Comprehensive bridge deck deterioration mapping of nine bridges by Non-destructive evaluation technologies.” Final Report, Iowa Department of Transportation, Report No. SPR-NDEB(90)--8H-00, November 2013.
- [16] Gucunski, N. et al., (2013). “Non-destructive testing to identify concrete bridge deck deterioration.” Report, Strategic Highway Research Program 2, Report No.S2-R06A-RR-1, November 2013.
- [17] Hema, J., Guthrie, W., Fonseca, F., (2004). “Concrete bridge deck condition assessment and improvement strategies.” Report, Utah Department of Transportation, Report No. UT-04-16, November 2013.
- [18] Hasan, H., Ramirez, J., Cleary, D., (1995). “Indiana evaluates epoxy-coated steel reinforcement.” Journal Article, Better Roads, Vol. 65, No. 5, pp. 21-25, November 2013.
- [19] Phares, B., Rolander, D., Graybeal, B., Washer, G., (2001). “Reliability of visual bridge inspection.” Journal Article, Public Roads, Vol. 64, No. 5, November 2013.
- [20] Missouri Department of Transportation (MoDOT), 2013. “Engineering polity guide.” Design Guide, Section 753.2, Missouri Department of Transportation. Jefferson City, MO, October 2013.
- [21] American Standard Test Method (ASTM) D 4580/ D 4580M, 2012. “Standard practice for measuring de-laminations in concrete bridge decks by sounding.” Standard, ASTM International, West Conshohocken, PA., November 2013.
- [22] Strategic Highway Research Program 2 (SHRP 2), 2013. “Hammer sound/ chain drag description.” Strategic Highway Research Program 2 ND Toolbox, <<http://www.ndtoolbox.org/content/bridge/cd-description>> November 2013.
- [23] Scott, M., et al. (2003). “A comparison of non-destructive evaluation methods for bridge deck assessment.” Journal Article, NDT&E International, Vol. 36, pp. 245- 255, November 2013.

- [24] Gucunski, N., Antoljak, S, Maher, Ali., (2000). "Seismic methods in post construction condition monitoring of bridge decks." Proceedings, Use of Geophysical Methods in Construction, pp. 35-51, November 2013.
- [25] Strategic Highway Research Program 2 (SHRP 2), 2013. "Ground penetrating radar description." Strategic Highway Research Program 2 NDTtoolbox, <<http://www.ndtoolbox.org/content/bridge/gpr-description> > November 2013.
- [26] Maser, K., (2009). "Integration of ground penetrating radar and infrared thermography for bridge deck condition evaluation." Proceedings, Non-Destructive Testing in Civil Engineering 2009, Nantes, France, November 2013.
- [27] Morrissey, J. (2013). "What is GPR?" Previous Research, <<http://johnpmorrissey.com/gpr.html>> November 2013.
- [28] Strategic Highway Research Program 2 (SHRP 2), 2013. "Ground penetrating radar physical principle." Strategic Highway Research Program 2 NDTtoolbox, <<http://www.ndtoolbox.org/content/bridge/gpr-physical-principle>> November 2013.
- [29] American Standard Test Method (ASTM) D 6087, 2008. "Standard test method for evaluating asphalt-covered concrete bridge decks using ground penetrating radar." Standard, ASTM International, West Conshohocken, PA., November 2013.
- [30] Geophysical Survey Systems, Inc. (GSSI), (2013). "Bridge deck condition assessments with GSSI GPR." Geophysical Survey Systems, Inc., <<http://www.geophysical.com/bridgeinspection.htm#nogo>> November 2013.
- [31] Yehia, S., Abudayyeh, O., Abdel-Qader I., Zalt, A., (2008). "Ground-penetrating radar, chain drag, and ground truth." Journal Article, Transportation Research Record, No. 2044, pp. 39-50, October 2013.
- [32] Strategic Highway Research Program 2 (SHRP 2), 2013. "Ground penetrating radar limitations." Strategic Highway Research Program 2 NDTtoolbox, <<http://www.ndtoolbox.org/content/bridge/gpr-limitations>> November 2013.
- [33] Arndt, R.W., Jalinoos, F., Cui, J., Huston, D., (2010). "Periodic NDE in support of structural health monitoring of bridges." Proceedings, Fifth International IABMA Conference, Philadelphia, USA, pp. 148, November 2013.
- [34] Federal Highway Administration (FHWA), (2013). "RABITTM Bridge Deck Assessment Tool." Federal Highway Administration, <<http://www.fhwa.dot.gov/research/tfhrc/programs/infrastructure/structures/lbtp/lbtltpresearbit/index.cfm>> December 2013.
- [35] American Standard Test Method (ASTM) C 42/C42M, 2013. "Standard test method for obtaining and testing drilled cores and sawed beams of concrete." Standard, ASTM International, West Conshohocken, PA., November 2013.

- [36] American Standard Test Method (ASTM) C 856, 2011. “Standard practice for petrographic examination of hardened concrete.” Standard, ASTM International, West Conshohocken, PA., November 2013.
- [37] American Standard Test Method (ASTM) C 1152, 2004. “Standard test method for acid-soluble chloride in mortar and concrete.” Standard, ASTM International, West Conshohocken, PA., November 2013.
- [38] American Standard Test Method (ASTM) C 1218, 1999. “Standard test method for water-soluble chloride in mortar and concrete.” Standard, ASTM International, West Conshohocken, PA., November 2013.
- [39] Kepler, J., Darwin, D., Locke, C. Jr., (2000). “Evaluation of corrosion protection methods for reinforced concrete highway structures.” Report, Structural Engineering and Engineering Materials, SM Report No. 58, November 2013.

VITA

Abhishek Kodi was born in Kakinada, Andhra Pradesh, in Southern India. He had a proclivity towards Physical Sciences since his High School. This fascinated him in pursuing an Integrated Master's degree in Earth Sciences, emphasizing in geology. He worked in diverse fields from palaeontology to climate sciences. He later enrolled in Missouri University of Science and Technology for another Master's degree in Geological/Geophysical Engineering. During his graduate program he met some very inquisitive people and learned valuable lessons in class and outside classrooms. He was awarded his MS degree in Geological Engineering in May 2016. Then he was off to chase his dreams.